[American Journal of Science, Vol. 322, December, 2022, P. 1089–1123, DOI 10.2475/10.2022.01]

American Journal of Science

DECEMBER 2022

ASSESSING THE LONG-TERM LOW-TEMPERATURE THERMAL EVOLUTION OF THE CENTRAL INDIAN BUNDELKHAND CRATON WITH A COMPLEX APATITE AND ZIRCON (U-TH)/HE DATASET

CODY L. COLLEPS*,**,†, N. RYAN MCKENZIE*, PETER VAN DER BEEK**, WILLIAM R. GUENTHNER***, MUKUND SHARMA§, ADAM R. NORDSVAN*, and DANIEL F. STOCKLI§§

ABSTRACT. **Modern approaches in low-temperature thermochronometry are capable of extracting long-term thermal histories from cratonic settings that may elucidate potential drivers of deep-time phases of intracontinental burial and erosion. Here, we assess the utilization of the Radiation Damage Accumulation and Annealing Model for apatite (RDAAM) and zircon (ZRDAAM) to track the long-term low-temperature thermal evolution of the Archean Bundelkhand craton and the surrounding undeformed strata of the ~1.7–0.9 Ga Vindhyan successions in central India. We correspondingly interpret a complex basement and detrital zircon and apatite (U-Th)/He (ZHe and AHe, respectively) dataset in light of observed model limitations and known geologic context. ZHe and AHe dates from across the craton reveal a significant (>300 Myr) date inversion between the two systems within grains with moderate to high effective uranium (eU) concentrations. Inverse thermal models utilizing current ZRDAAM and RDAAM parameters are not capable of reproducing observed coupled basement ZHe and AHe data for the same thermal history. However, meaningful thermal information can be extracted from AHe inverse models coupled with a forward modeling approach applied to detrital ZHe data from Vindhyan deposits, which have notably lower eU concentrations and yield significantly older ZHe dates (between ~1,475 and 575 Ma) than basement zircon. Resulting thermal models indicate that the Bundelkhand craton experienced peak burial temperatures of ~150°C between 850 and 475 Ma, followed by a major crustal cooling event at ~350–310 Ma, possibly driven by late Paleozoic glaciations and/or epeirorogenic uplift. Inverse models including AHe data require a Deccan Traps related thermal perturbation between ~66 and 65 Ma, and we suspect that this event overprinted basement zircon with moderate to high eU concentrations. Although the effects of zonation, grain morphology, and/or uncertainties in damage-annealing parameters contribute to disparities between predicted and observed AHe and ZHe dates, these factors alone cannot account for the major ZHe and AHe date inversion observed from the Bundelkhand craton. Instead, it is likely the case that current damage-dependent models for ^{4}He diffusion are not adequately calibrated at the resolution necessary to predict short-lived thermal perturbations that occurred in a late phase relative to a prolonged period of extensive damage accumulation.**

Key words: Thermochronology, (U-Th)/He, Radiation Damage, Craton, India, Deccan Traps Late Paleozoic Glaciation

* Department of Earth Sciences, University of Hong Kong, Pokfulam, Hong Kong
** Institute of Geosciences, University of Potsdam, Potsdam-Golm, Germany
*** Department of Geology, University of Illinois at Urbana-Champaign, Urbana, IL, USA
§ Birbal Sahni Institute of Palaeosciences, Lucknow, India
§§ Department of Geological Sciences, Jackson School of Geosciences, University of Texas at Austin, TX, USA
† Corresponding author: colleps@uni-potsdam.de

INTRODUCTION

Though far removed from modern plate boundaries, ancient continental interiors may experience complex evolutions with multiple phases of burial, erosion, and magmatism that may be reflected in their long-term thermal histories. The weathering and erosion of crustal rocks throughout Earth's history has direct and sizable impacts on the Earth system, from influencing broad-scale tectonic and magmatic processes (for example, Keller and others, 2019; Sobolev and Brown, 2019), to modulating Earth's deep-time carbon cycle (for example, Berner and others, 1983; Lee and others, 2018). It is thus imperative to understand and directly constrain erosional processes at a multitude of spatial and temporal scales. The mechanisms responsible for episodes of burial and erosion within long-lived cratons remain intensely debated (for example, Flowers and others, 2020; Flowers and others, 2022; McDannell and others, 2022), and discriminating between tectonic, climatic, and/or epeirogenic drivers of deep-time crustal erosion at regional and global scales remains a challenge that requires robust, high-resolution, and prolonged low-temperature thermal histories from multiple cratonic settings to resolve. Tracking craton thermal histories is also vital to improve our understanding of the drivers that control the relative vertical motions within tectonically quiescent settings over prolonged (that is, 100–1000 Myr) timescales (for example, DeLucia and others, 2017; McDannell and others, 2018).

Recent advances in low-temperature thermochronometry permit the extraction of deep-time thermal information from cratonic rocks and basin sediments, from which long-term thermal histories may be interpolated with various degrees of confidence (for example, Kohn and Gleadow, 2019). The capability to model complex, long-term thermal histories is in part a result of the development of the Radiation Damage Accumulation and Annealing model for both the apatite (U-Th)/He (AHe) (RDAAM; Flowers and others, 2009) and zircon (U-Th)/He (ZHe) (ZRDAAM; Guenthner and others, 2013) systems. These models account for the impact of radiation damage accumulation on single-crystal He diffusivities. Whereas thermal histories derived from these techniques have been utilized to assess potential mechanisms for crustal cooling at varying spatial scales (Orme and others, 2016; DeLucia and others, 2017; Guenthner and others, 2017; Mackintosh and others, 2017; Baughman and Flowers, 2020; Flowers and others, 2020; Peak and others, 2021; Thurston and others, 2022; McDannell and others, 2022), the broader implications of these models remain incompletely explored due to (1) the current lack of global-scale perspectives in crustal erosion within cratons, and (2) known discrepancies in damage-dependent ^{4}He diffusion kinetics that may negate the uniqueness of current thermal history models. Here, we expand the application of low-temperature thermochronometry to central India, and we evaluate the capabilities and limitations of modern thermochronometric techniques to extract meaningful thermal information from a complex AHe and ZHe dataset from the Archean Bundelkhand craton and its marginal Proterozoic basins.

The ~3.4–2.5 Ga Bundelkhand craton, located within the continental interior of central India, provides a unique setting to extract long-term thermal histories with the motivation to assess potential drivers for baseline continental burial and erosion. This setting is particularly unique for this baseline assessment, as correlative, flat-lying Proterozoic deposits of the Vindhyan succession are observed in direct nonconformable contact with the Bundelkhand basement on both the western and eastern craton margin, separated by ~250 km (Ray, 2006; Meert and Pandit, 2014; Bose and others, 2015; Shukla and others, 2019) (fig. 1A). The undeformed nature of these deposits indicate that the Bundelkhand region has not been directly affected by tectonism for over a billion years (for example, Chakrabarti and others, 2007), and thus burial and erosion within central India since the Proterozoic is likely epeirogenically and/or

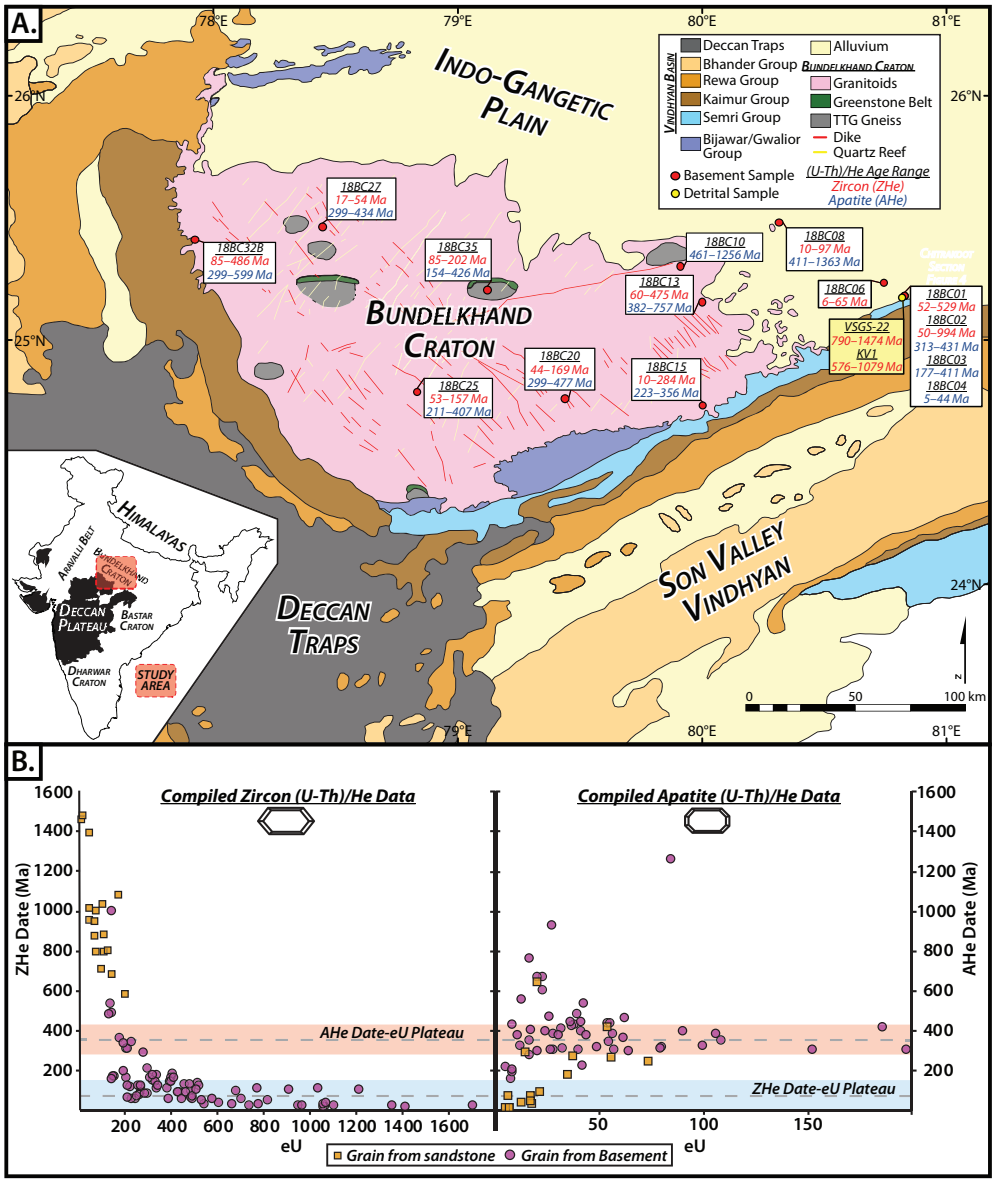

Fig. 1. (A) Lithological map of the Bundelkhand craton region with sample locations, and (B) compiled apatite and zircon (U-Th)/He data. The observed range of AHe and ZHe dates is listed for each sample locality. Sandstones from the Vindhyan successions analyzed for detrital ZHe dates were collected from the Sangrampur hillock along the northeastern craton margin. Date-eU plots for the compiled ZHe and AHe dataset reveal a distinct reversal in AHe and ZHe dates at moderate to high eU values. Analyzed apatite and zircon grains from Vindhyan sandstones yield anomalously low eU values, resulting in significantly older ZHe dates and younger AHe dates compared to basement data.

climatically induced. A previous study utilizing RDAAM and AHe dates broadly constrained the Phanerozoic thermal evolution of the eastern craton margin, and indicated that the Deccan Traps large igneous province (LIP) volcanism thermally perturbed this region despite its location ~200 km northeast of the northernmost preservation of Deccan Traps flood basalts within the Malwa Plateau (Colleps and

others, 2021a). This study expands on the previously published AHe dataset from the eastern craton, and incorporates a new, notably complex AHe and ZHe dataset from across the craton, as well as from Vindhyan sediments in direct nonconformable contact with the basement.

We exploit this complex basement and detrital dataset to comprehensively assess coupling RDAAM and ZRDAAM for deep-time thermal history modeling and explore various factors (for example, U and Th zonation, differing damage annealing kinetics, Deccan Trap reheating) that may contribute to observed data and model disparities. With the newfound insight into damage-diffusivity relationships observed in the coupled AHe and ZHe datasets, we apply a hybrid inverse and forward modeling approach to best constrain the long-term low-temperature thermal evolution of the Bundelkhand region. We interpret resulting thermal histories in light of known model limitations and discuss the potential mechanisms responsible for observed deep-time phases of crustal cooling and heating in the context of regional- and global-scale geodynamic and climatic processes.

RADIATION DAMAGE ACCUMULATION AND ANNEALING MODELS FOR THE ZIRCON AND APATITE (U-TH)/HE SYSTEMS

Low-temperature (U-Th)/He thermochronometry is centered around the thermally activated diffusion of radiogenic helium out of the crystal lattice of various U and Th bearing accessory minerals (Dodson, 1973; Zeitler and others, 1987; Reiners and others, 2002). A thorough understanding of helium diffusion kinetics in naturally occurring accessory minerals provides a means to track the thermal evolution of various geologic settings within a given temperature range. It is well known that the amount of radiation-damage accumulation within these minerals can significantly increase and/or decrease helium diffusivities of a given system (Shuster and others, 2006; Flowers and others, 2007; Gautheron and others, 2009; Shuster and Farley, 2009; Guenthner and others, 2013; Ketcham and others, 2013; Anderson and others, 2017), and ZRDAAM and RDAAM use empirically derived diffusivities from a suite of samples with varying amounts of radiation damage to address this effect for the ZHe and AHe systems, respectively (Flowers and others, 2009; Guenthner and others, 2013) (fig. 2A). These models utilize effective uranium concentrations (eU = U + 0.235 × Th) and fission-track annealing properties as a proxy to track the susceptibility of individual grains to the accumulation and annealing of radiation damage, which is dependent on the duration spent at or below annealing temperatures. One major caveat to conventional ZRDAAM and RDAAM is that they utilize fission-track kinetics as a direct proxy for radiation damage accumulation and annealing. It is well understood that fission-track retentivity is influenced by radiation damage and that fission-track kinetics only partially reflect the complexities of heterogenous damage accumulation and annealing (Willett and others, 2017; Ginster and others, 2019; Guenthner, 2021). Despite these complexities, the fission-track-based kinetics of ZRDAAM and RDAAM still provide a suitable first-order proxy for radiation damage, and we explore the utility of various damage kinetic models in the discussion.

For the AHe system, RDAAM defines an increase in ^{4}He retentivity with increasing radiation damage, resulting in positive date-eU trends that can vary significantly depending on differing time-Temperature (t-T) histories (Flowers and others, 2009) (fig. 2A). Similarly, ZRDAAM predicts date-eU trends for unique t-T histories, although these trends often yield an initial positive date-eU correlation at low to moderate damage levels that eventually switches to a negative correlation at higher eU (Guenthner and others, 2013). These relationships are interpreted to reflect increased ^{4}He retentivity at low to moderate eU as the result of accumulated damage "blocking" the fast diffusion c-axis until a threshold is met, resulting in an interconnected network of damage

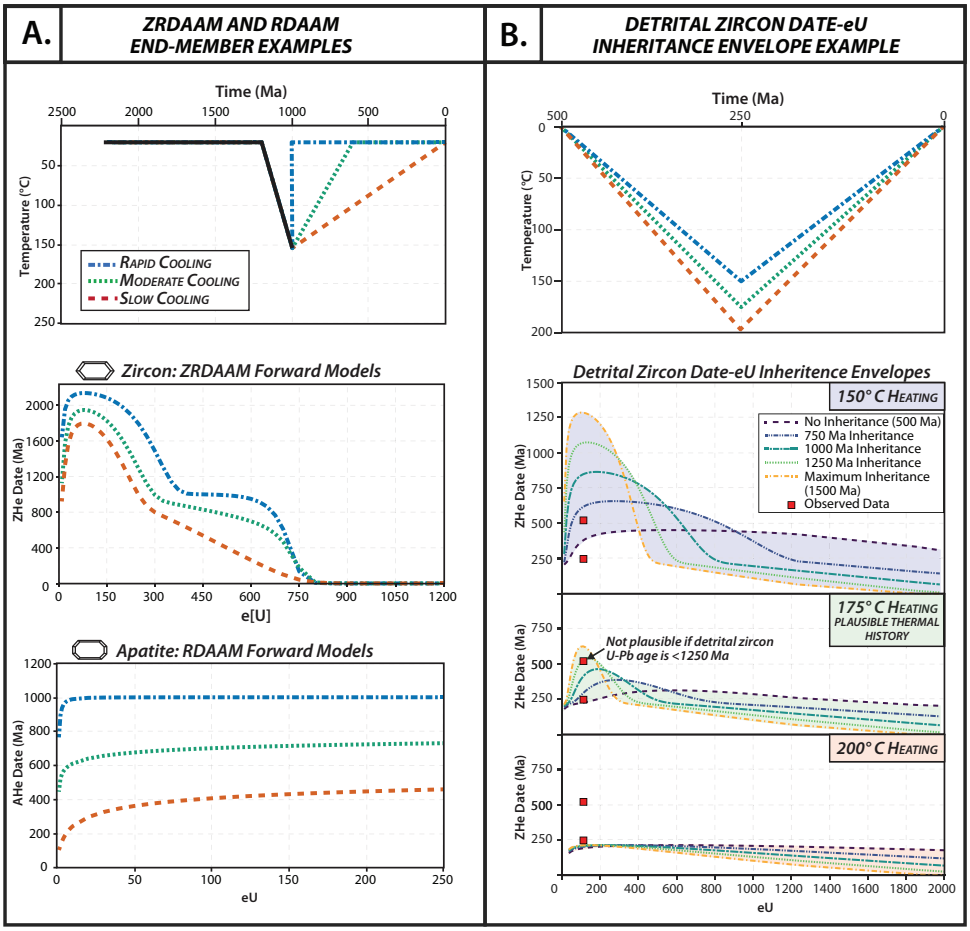

Fig. 2. Schematic diagrams illustrating (A) ZRDAAM and RDAAM ZHe and AHe date predictions for differing thermal histories, and (B) the detrital ZHe date-eU inheritance envelope forward modeling approach. (A) AHe and ZHe date-eU forward-model results predicted with RDAAM and ZRDAAM, respectively, for three end-member thermal histories that involve extensive zircon damage accumulation since 2200 Ma, followed by burial at 1200 Ma, and the initiation of slow, moderate, or rapid cooling at 1000 Ma. The shape of a given date-eU curve is highly dependent on the thermal evolution experienced by a sample. These forward models reveal the impact of radiation-damage accumulation and annealing on He diffusivities and observed AHe and ZHe dates. (B) Detrital zircon date-eU inheritance envelopes are plotted for three simple burial and unroofing thermal histories from 500 Ma to the present with varying degrees of burial (to 150°C, 175°C, and 200°C) at 250 Ma. These inheritance envelopes take into account the likeliness that detrital zircons from a sandstone—particularly one which has not experienced temperatures greater than ~220°C since deposition—will contain inherited concentrations of ^{4}He reflective of their pre-depositional thermal evolution. This example shows date-eU plots for a zircon with zero ^{4}He inheritance (that is, has a ZHe date of 0 My at the time of deposition), a maximum ^{4}He inheritance (assumed based on a hypothetical oldest detrital zircon U-Pb age of 1500 Ma), and intermediate ^{4}He inheritances of 750, 1000, and 1250 Ma; upper and lower limits of these compiled date-eU curves signify the permissible inheritance envelope. The ^{4}He inheritance modeled here from 500–1500 Ma assumes that a detrital zircon remained at surface temperatures from a given inheritance date until the time of deposition (in this case at 500 Ma). For a given thermal history to be considered plausible, observed detrital ZHe data must lie within the permissible inheritance envelope, such as shown in the detrital ZHe date-eU plot for the scenario with burial to 175°C. Notably, an individual detrital ZHe data point must lie within a maximum date-eU inheritance envelope equivalent to its detrital zircon U-Pb age—it is advantageous to have both a U-Pb and ZHe date for a single grain as an additional constraint. All forward models assume an average grain size of 50 microns.

induced fast-diffusion pathways, which significantly increases ^{4}He diffusivities (Ketcham and others, 2013). Observed date-eU trends are highly dependent on t-T histories, grain size, and zonation of uranium and thorium. Accordingly, RDAAM and ZRDAAM can obtain meaningful thermal histories from ZHe and AHe datasets that yield significant date disparities but possess distinct date-eU relationships. We consider all single-grain ZHe and AHe dates with a radiation damage-influence to reflect "apparent ages" resulting from a dynamic geological history of radiation damage accumulation, heating, and cooling. For clarity and simplicity, however, we refer to all single-grain and compiled data throughout this paper in reference to its "date" (calculated from measurements) as opposed to an "age" (the interpretation of the date) (for example, Dutton and others, 2017), because single AHe or ZHe dates cannot always be interpreted to reflect specific geologic events for reasons discussed above.

In individual samples (or a compiled suite of samples) where it can be adequately assumed that all grains have experienced the same thermal history since complete damage annealing, inverse and forward thermal history modeling provide a relatively straightforward approach to interpret t-T pathways that may predict observed date-eU relationships (fig. 2A). Applying RDAAM and ZRDAAM to detrital samples with grains of varying degrees of inherited partial resetting adds complexities that render extracting useful thermal histories from such datasets more challenging (Guenthner and others, 2015; Powell and others, 2016; Fox and others, 2019; Pujols and others, 2020) (fig. 2B). This complexity arises because each individual detrital grain may have undergone a unique pre-depositional history that preserves a specific "inherited" amount of helium and damage accumulation in each grain. However, this radiation damage and helium inheritance effect for partially reset detrital grains can be accounted for using date-eU inheritance envelopes (Guenthner and others, 2015) (fig. 2B). This approach involves forward modeling date-eU curves for zero helium inheritance grains (that is, ZHe or AHe date of 0 Ma at time of deposition) and for grains with preceding helium inheritances as assumed by adding an extended period of time at surface temperatures prior to the sample's post-depositional history. The maximum allotted helium inheritance can be constrained based on the sample's oldest detrital grain, such that the maximum inheritance ZHe date-eU curve reflects a grain that has been at or near-surface temperatures since crystallization until its final deposition. Accordingly, observed data that lie within the date-eU inheritance envelope (zero inheritance to oldest crystallization inheritance) for a given t-T pathway provide a plausible post-depositional thermal history experienced by a detrital sample (fig. 2B).

Providing both a U-Pb crystallization age and a (U-Th)/He age for a single detrital grain (U-Pb-He double dating) (Reiners and others, 2005) allows further refinement in the utilization of date-eU inheritance envelopes. First, the area of the date-eU inheritance envelope can be reduced as an assumed maximum inheritance can be eliminated—the maximum inheritance cannot exceed the oldest observed U-Pb age in the dataset. Secondly, when a detrital zircon has a U-Pb age significantly younger than the oldest observed U-Pb age in its population, the oldest date-eU inheritance constraint cannot apply to the younger grain. In other words, double-dated zircons permit constraining the maximum inheritance for each grain, which provides an additional discriminatory characteristic that considerably reduces uncertainties and improves the resolution of thermal models.

GEOLOGIC SETTING

The Bundelkhand craton of central India is predominantly composed of ~2.6–2.5 Ga granitoids, with sparsely preserved Archean greenstone belts and ~3.6–3.3 Ga tonalite–trondhjemite–granodiorite gneisses (Kaur and others, 2014; Kaur and others, 2016; Joshi and others, 2017; Slabunov and Singh, 2019) (fig. 1). Craton assembly was completed by ~2.5 Ga, followed by broad-scale exhumation through mid-crustal

depths from ~2.4 to 2.3 Ga. This exhumation was inferred from near-uniform ~2.4 to 2.3 Ga apatite U-Pb dates observed across the craton (Colleps and others, 2021b), which indicate that this region has remained at temperatures below ~350°C since ~2.3 Ga. The craton was buried by ~2.2 Ga with the onset of Gwalior and Bijawar group deposition along the northwest and southeast craton margins, respectively (Colleps and others, 2021b). Near-horizontal strata of the Proterozoic Vindhyan successions unconformably overlie moderately dipping beds of the Paleoproterozoic Gwalior and Bijawar groups where they are preserved (Crawford and Compston, 1969; Chakraborty and others, 2015), although the Vindhyan strata are more commonly in direct nonconformable contact with the Bundelkhand craton along its eastern and western margins (fig. 1).

The Vindhyan Supergroup is subdivided into the Lower and Upper Vindhyan successions by a major unconformity between the ~1.7–1.6 Ga Lower Vindhyan Semri Group and the ~1.2–1.1 Ga Upper Vindhyan Kaimur Group (Chakrabarti and others, 2007; McKenzie and others, 2011; Bose and others, 2015; Colleps and others, 2021b). Included in the Upper Vindhyan succession is the Rewa Group (stratigraphically above the Kaimur Group) and the Bhander Group composed of the youngest rocks within the Vindhyan successions (Adnan and Shukla, 2014; Verma and Shukla, 2015) (fig. 1). Whereas the age constraints for the uppermost Vindhyan deposits remain debated, a compilation of detrital zircon ages from the Kaimur, Rewa, and Bhander groups suggest a maximum depositional age of ~900 Ma (Malone and others, 2008; McKenzie and others, 2011; Turner and others, 2014; Colleps and others, 2021b). Within the Son Valley Vindhyan successions, this maximum depositional age is broadly consistent with a Pb-Pb age of 908 ± 72 Ma from the Bhander Limestone (Gopalan and others, 2013). Immediately south of the Bundelkhand craton, flood basalts of the ~66–65 Ma Deccan Traps onlap Vindhyan strata at varying stratigraphic horizons (Schöbel and others, 2014; Schoene and others, 2015) (fig. 1). Deccan basalts may have once overlain the Bundelkhand region >150 km north of their present-day preservation and have since eroded (Colleps and others, 2021a). The northern portion of the craton is covered by Gangetic alluvium, and rivers drain north across the craton into the eastward flowing Yamuna River. Accordingly, there is a significant hiatus between the Vindhyan strata and Deccan flood basalts to the south and Gangetic alluvium to the north—little can be derived on the Phanerozoic burial and erosional evolution of central India from the stratigraphic record.

The eastern Bundelkhand craton is unconformably overlain by the Lower Vindyan Semri Group, whereas the Upper Vindhyan Kaimur Group is in direct contact with Bundelkhand basement along the western margin. The disconformity between the Semri and Kaimur Groups is well exposed along the eastern margin (Kumar and Sharma, 2012; Shukla and others, 2019). In some localities, such as the Sangrampur hillock near Chitrakoot in the northeast (fig. 1), a condensed section of the Semri Group is preserved, and both the nonconformity between Semri Group and the craton, and the disconformity between the Semri and Kaimur groups are exposed within ~30–50-meter-thick sections (Colleps and others, 2021a; Colleps and others, 2021b). These condensed sections (for example, Sangrampur hillock) are particularly important, as it can be assumed that the exposed basement, Semri Group, and Kaimur Group rocks at these locations experienced the same thermal evolution since Kaimur deposition. Thus, these sections provide important constraints for thermal modeling, as the craton was at or near-surface temperatures by ~1.2–1.1 Ga, followed by burial beneath the Rewa and Bhander groups, and perhaps a younger burial event no longer preserved in the stratigraphic record. Utilizing ZHe and AHe data from Vindhyan deposits and the Bundelkhand craton with RDAAM and ZRDAAM provides a means to assess (1) maximum burial temperatures of the craton since Kaimur deposition, (2) when the craton last experienced maximum burial, and (3) when/how the craton and surrounding basin rocks were exhumed to the surface.

METHODS

Sampling, Testing, and Predictions

A total of 11 samples from across the Bundelkhand craton were analyzed for ZHe dates. This study presents new AHe data from eight samples collected across the craton, which are compiled with published AHe data from five samples along the eastern craton margin (Colleps and others, 2021a). In addition, two samples from Vindhyan deposits (one each from the Semri and Kaimur groups) atop the Sangrampur hillock were analyzed for detrital zircon U-Pb-He double dating. The diversity of this dataset provides a unique opportunity to test modern approaches to constrain long-term thermal histories from cratonic interiors. Under the assumption that ZRDAAM and RDAAM are adequately calibrated, we could expect to extract thermal histories that satisfy the observed compiled basement ZHe and AHe dataset and the detrital ZHe dataset (with date-eU inheritance envelopes). To test this assumption, we utilize coupled inverse and forward thermal history modeling techniques that account for varying sources of uncertainty, and we directly compare observed data with model predictions to scrutinize the capabilities and limitations in applying damage-diffusivity dependent models to constrain deep-time thermal histories.

Analytical Procedures

All (U-Th)/He analyses were conducted at the UTChron facilities at the University of Texas at Austin, following the analytical procedures of Wolfe and Stockli (2010). For each basement sample, ~6 apatite crystals and 8–10 zircon crystals were analyzed for (U-Th)/He dates, with inclusion free, euhedral crystals selected when possible. When selecting zircon for analyses, radiation damage was first qualitatively assessed based on grain color and opaqueness—a range of grains with varying visually assessed damage were chosen to increase the likeliness of generating data over a broad range of eU values (Ault and others, 2018). Each crystal was photographed, morphometrically measured for alpha-ejection corrections, and placed in ~1 mm platinum packets prior to analysis. Packed samples were placed in an ultra-high vacuum helium extraction line and degassed by heating via a diode laser. Extracted gas was purified, and helium concentrations were obtained by isotope dilution and $^{3}He/^{4}He$ measurement using a quadrupole mass spectrometer. Once degassed, samples were spiked and dissolved using standard procedures for apatite and zircon dissolution, and U, Th, and Sm concentrations were measured using a ThermoElement2 inductively coupled plasma mass spectrometer. With known ^{4}He, U, Th, and Sm concentrations, a raw date was calculated, and an alpha-ejection correction was applied to derive corrected (U-Th)/He dates. A uniform uncertainty based on the intralaboratory reproducibility of standards (6% for Durango apatite and 8% for Fish Canyon Tuff zircon) was applied to each individual corrected date.

Double-dated detrital zircon were analyzed for U-Pb before the standard (U-Th)/He analyses. For each sample, ~15 whole detrital zircon grains were placed on an epoxy mount with double-sided sticky tape, and unpolished zircons were analyzed for U-Pb ages via laser ablation ICP-MS at the UTChron facilities at the University of Texas at Austin. The resulting U-Pb ages were compiled and published in a broader U-Pb study (Colleps and others, 2021b), and ~8–9 grains with concordant U-Pb ages from each sample were selected to obtain detrital ZHe dates.

RESULTS

Craton ZHe and AHe Results

Compiled ZHe data from all Bundelkhand basement samples range between 134 and 1710 ppm in eU concentrations, with ZHe dates ranging from 6 to 994 Ma

(fig. 1B). Compiled AHe data from the Bundelkhand craton range between 5 and 198 ppm in eU concentrations; AHe dates range from 5 to 1363 Ma with a majority of high eU grains ranging between ~300 and 450 Ma (fig. 1B). All samples were subdivided into the following groups based on their geographic position and observed ZHe and AHe data similarities: western craton, central craton, northeastern craton, and eastern craton margin (fig. 3). All data tables with detailed sample information are provided in the supplementary information.

Within the western craton group, sample 18BC32B was collected at the western craton margin directly beneath the Upper Vindhyan Kaimur Group, and sample 18BC27 was collected ~50 km east of the margin (fig. 1A). Compiled ZHe results (N=2; n=16) from these basement rocks reveal a strong negative date-eU relationship, with ZHe dates ranging from 486 Ma to 17 Ma with moderate to high eU values of 144–968 ppm (fig. 3A). Compiled AHe results (N=2; n=12) from these samples yielded a relatively flat date-eU relationship, with AHe dates ranging between 300 and 599 Ma for eU values between 13 and 100 ppm and an average AHe date of 375 Ma (fig. 3B).

Two samples from the central craton group (18BC25; 18BC35) yielded ZHe dates between 64–202 Ma, eU values ranging from 301 to 706 ppm, and a distinct negative date-eU relationship (N=2; n=18) (fig. 3C). Compiled AHe dates range from 154–426 Ma with eU values ranging from 5–40 ppm (N=2; n=12) (fig. 3D). A positive date-eU relationship is present at eU values of 5–15 ppm, and single-grain AHe dates with eU >15 ppm are relatively consistent with an average AHe date of 339 Ma (n=6) (fig. 3D).

Samples from the northeastern craton group yielded significantly older AHe dates when compared to the craton as a whole, and we accordingly categorized these samples separately. Samples 18BC08 and 18BC13 were analyzed for ZHe data, and compiled results reveal a subtle negative date-eU trend with ZHe dates between 10–475 Ma and eU values of 134–1710 ppm (N=2; n=15) (fig. 3E). Compiled data from samples 18BC08, 18BC10, and 18BC13 have AHe dates between 382 and 1363 Ma and eU values between 8 and 85 ppm (N=3; n=17) (fig. 3F). Compiled AHe data do not reveal a significant date-eU relationship, although single-grain results from sample 18BC08 reveal a particularly steep positive date-eU trend (fig. 3F).

This study builds upon a published AHe dataset from the eastern craton margin group (Colleps and others, 2021a); five new samples from this region were analyzed for ZHe data. Samples 18BC01 and 18BC02 were collected from a doleritic dike and granitoid, respectively, from the Sangrampur hillock along the northeastern margin, ~15 meters beneath exposed Vindhyan deposits (fig. 4). Sample 18BC06 was collected ~8 km northwest of the Sangrampur hillock, sample 18BC15 was collected directly beneath Vindhyan deposits ~90 km southwest of the Sangrampur hillock, and sample 18BC20 was collected ~50 km west of the craton margin and 18BC15. Compiled dates from these samples provide the highest-resolution ZHe dataset with a broad range of ZHe dates from 6–994 Ma with eU values of 143–1415 ppm (N=5; n=35) (figs. 3G and 4). A steep negative date-eU trend exists between eU values of ~150–400 ppm, and ZHe dates are relatively consistent at eU values >400 ppm with an average ZHe date of 58 Ma (n=16). Compiled AHe data from the eastern craton margin are from three Bundelkhand granitoid samples (18BC02; 18BC15; 18BC20), and two detrital samples from the basal Semri Group (18BC03) and Kaimur Group (18BC04) groups preserved within a condensed ~15–20-meter section atop the Sangrampur hillock in direct contact with the Bundelkhand craton. These AHe data from the Vindhyan succession were compiled with basement data under the assumption that (1) these rocks shared an identical thermal evolution since Kaimur deposition (~1.2–1.1 Ga), and (2) all apatite were completely reset and annealed sometime after their deposition (Colleps and others, 2021a). Compiled data provided AHe dates ranging from 5–641 Ma with eU

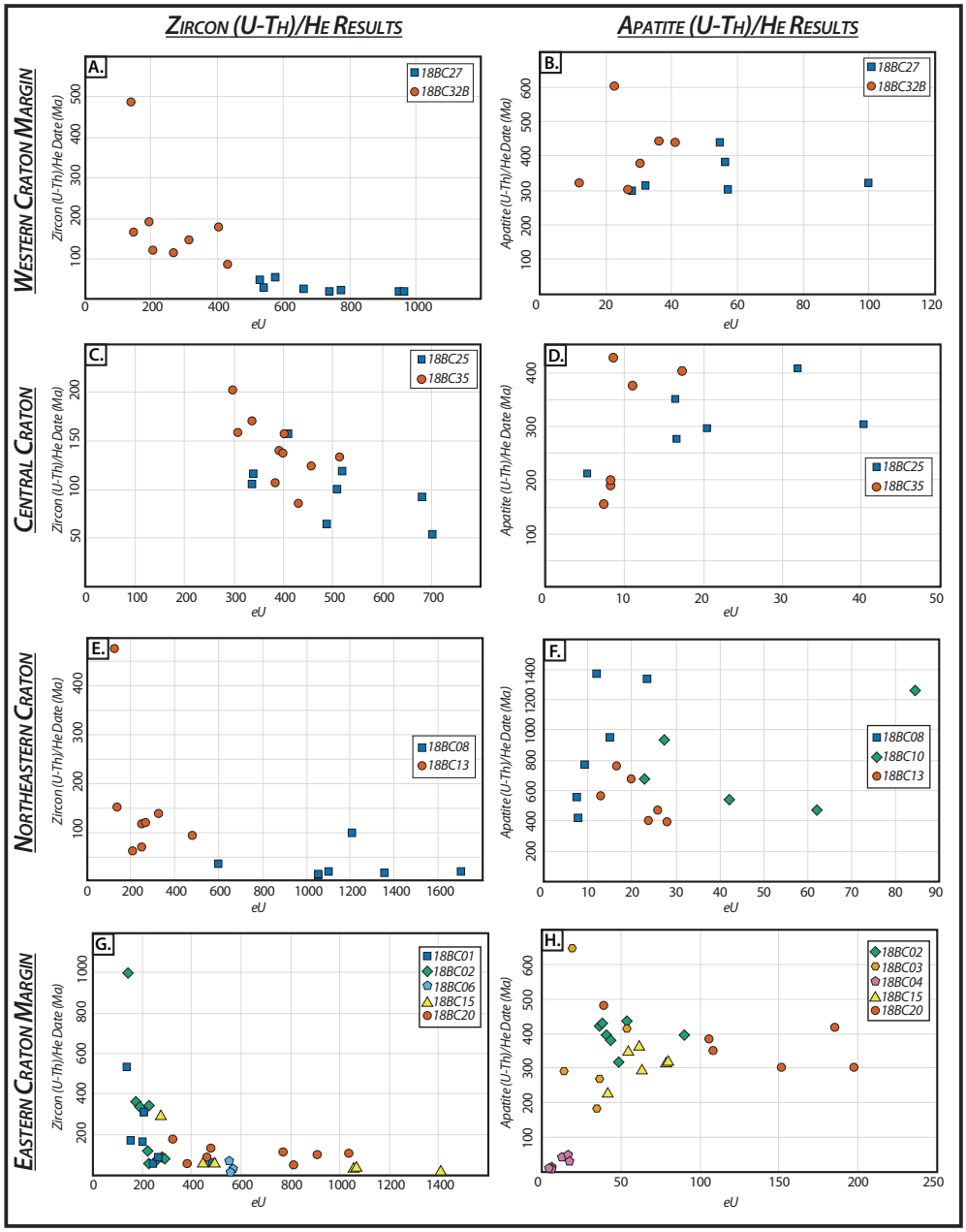

Fig. 3. Compiled basement ZHe and AHe date-eU plots sorted by geographic position within the Bundelkhand craton (e–h). All localities reveal distinct negative ZHe date-eU trends, whereas samples from the central craton region and the eastern craton margin show positive AHe date-eU trends. Compiled AHe and ZHe data from each region within the craton were coupled for inputs in HeFTy for inverse thermal history modeling; however, in every inverse modeling scenario, ZRDAAM and RDAAM could not adequately predict both AHe and ZHe datasets simultaneously. As a result, we utilized compiled data from the eastern craton margin—where both the largest dataset and the most robust geologic constraints exist—for an alternative modeling approach to extract plausible thermal histories and assess discrepancies in coupling the kinetics of ZRDAAM and RDAAM.

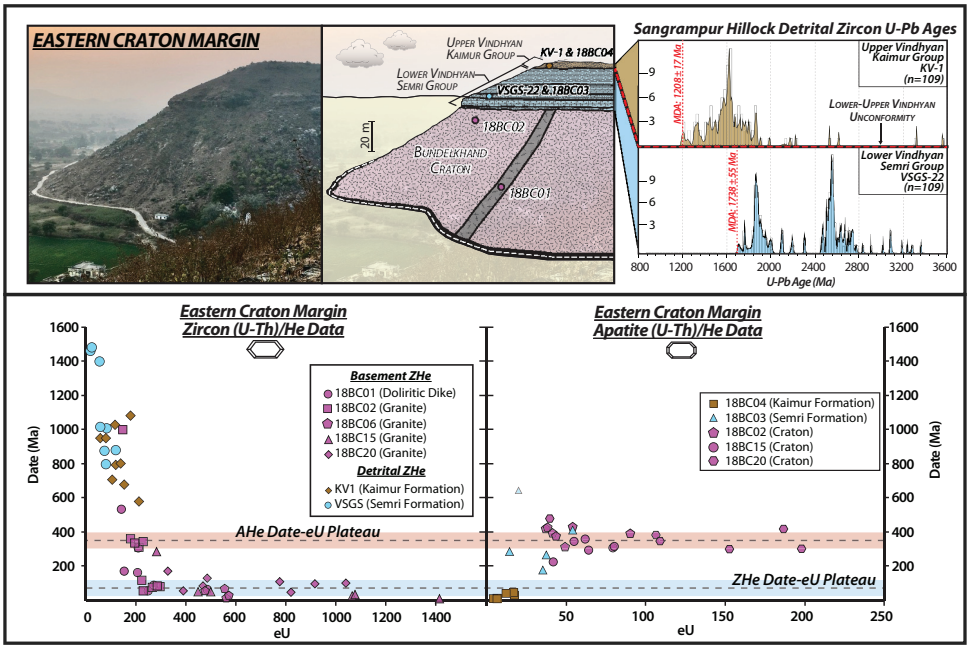

Fig. 4. Compilation of detrital zircon U-Pb, ZHe, and AHe data from the eastern craton margin, with an annotated photo of the Sangrampur hillock denoting sample localities and stratigraphic relationships. Detrital zircon ages were compiled from Colleps and others (2021b) and reveal the two following unconformities within ~30 meters: (1) nonconformity between the ~2.5 Bundelkhand granitoid and the 1.7 Ga Semri Group above it; (2) disconformity between the ~1.7 Ga Semri Group and pebbly conglomerate of the ~1.2 Ga Kaimur Group. The date-eU plots show compiled ZHe and AHe data from the eastern Bundelkhand craton margin, including detrital ZHe dates from sandstones of the Lower Vindhyan Semri Group and Upper Vindhyan Kaimur Group. Detrital ZHe dates from the Semri and Kaimur groups are older and have lower eU concentrations compared to ZHe data from the Bundelkhand granitoids immediately beneath. The oldest detrital ZHe date of ~1500 Ma indicates that the Bundelkhand craton has not experienced temperatures exceeding ~200°C since at least 1500 Ma. These older detrital ZHe dates preserve imperative thermal information that is effectively missing from the basement ZHe record. AHe data from the eastern craton margin were utilized in previously published inverse thermal history models (Colleps and others, 2021a). These thermal models were used to forward model detrital ZHe date-eU inheritance envelopes for direct comparison to observed detrital ZHe data from the Sangrampur hillock.

values of 5–198 ppm (N=5; n=30) (figs. 3H and 4). A steep positive date-eU curve is revealed at low eU values between ~5 and 50 ppm, and a date-eU plateau at ~350 Ma exists at eU values >50 ppm.

Detrital U-Pb-He Double Dating Results

At the Sangrampur hillock along the northeastern craton margin, a sandstone sample from the Lower Vindhyan Semri Group (VSGS) and a sandstone sample from the Upper Vindhyan Kaimur Group (KV-1) were analyzed for U-Pb-He double dates collected within a ~15-meter-thick section—a disconformity separates the two stratigraphic horizons (fig. 4). At this locality, the Semri Group is in direct nonconformable contact with the Bundelkhand Craton (samples 18BC01 and 18BC02). Detrital zircon age populations from these horizons at the Sangrampur hillock indicate a maximum depositional age of ~1.7 Ga for the Semri Group sandstone, and ~1.2 Ga for the Kaimur Group sandstone (Colleps and others, 2021b) (fig. 4). Detrital zircon analyzed for U-Pb-He from the Semri Group (n = 8) yield U-Pb ages ranging from 2430 to 3323 Ma, and ZHe dates from 790–1474 Ma. Kaimur Group detrital zircon (n = 9)

yield U-Pb ages of 1381–1887 Ma with ZHe dates ranging from 576–1079 Ma. Notably, detrital ZHe dates from the Sangrampur hillock are significantly older and yielded anomalously lower eU values (~10–200 ppm) than those directly from basement rock (fig. 1B).

THERMAL HISTORY MODELING

Inverse Thermal Modeling

To assess the long-term thermal evolution of central India, we first utilized a Monte Carlo based inverse modeling approach using observed data from basement samples and the HeFTy computer program (Ketcham, 2005). HeFTy incorporates the diffusion kinematics of RDAAM and ZRDAAM for the AHe and ZHe systems respectively, predicts thermochronometric results for randomly simulated t-T pathways, and statistically determines "good" and "acceptable" t-T pathways based on goodness of fit (GOF) parameters of >0.5 and >0.05, respectively. One limitation of HeFTy is that it allows a maximum of 7 individual data inputs (ZHe and/or AHe inputs in this case) for each simulation, such that a strategic approach is necessary to determine the most appropriate inputs for inverse modeling. A common and well-utilized approach when applying RDAAM and ZRDAAM is to filter and bin ZHe and AHe data appropriately based on their date-eU relationships and input the resulting average uncorrected date, U-Th concentrations, and grain size for each predetermined bin (Ault and others, 2013; DeLucia and others, 2017; Guenthner and others, 2017; Baughman and Flowers, 2020; Colleps and others, 2021a). Following this approach, coupled AHe and ZHe data from each defined geographic region were binned into 7 synthetic grain inputs based primarily on eU concentrations that best represent the first-order date-eU trend (Supplementary fig. S1).

The most robust thermal models are those capable of reproducing observed thermochronometric dates from multiple systems (for example, McDannell and others, 2019). Unfortunately, when coupling observed ZHe and AHe data from the Bundelkhand craton binned synthetic grain inputs into HeFTy with ZRDAAM and RDAAM kinetics, no "good" or "acceptable" fits result. This outcome was found for all simulations from all localities, even after applying various binning strategies, exploring initial geologic conditions (constraint boxes), and inputting differing combinations of binned AHe and Zhe data (Supplementary figs. S1 and S2). At first order, this indicates that a significant discrepancy exists in the empirically derived kinetics of RDAAM and/or ZRDAAM. Whereas numerous studies have utilized this approach to produce long-term t-T thermal histories that satisfy AHe, ZHe, and fission-track datasets, the inability of RDAAM and ZRDAAM to adequately predict our dataset in any scenario is unexpected. Accordingly, a modified approach was necessary to extract meaningful information for the complete ZHe and AHe dataset from central India regarding its thermal evolution (fig. 5).

Alternative Modeling Approach

One striking observation when assessing a compilation of detrital versus basement ZHe data from central India is the stark difference in ZHe dates and eU values. All detrital samples have significantly lower eU concentrations and older ZHe dates when compared to those from the craton (figs. 1 and 4). Given that lower eU concentrations are likely to result in minimal damage accumulation over prolonged periods, thus yielding higher closure temperatures, these observed detrital ZHe dates most likely indicate that the Bundelkhand craton has not been buried to temperatures hot enough to entirely reset the ZHe system since ~1475 Ma—the oldest observed detrital ZHe date. Accordingly, ZHe date-eU inheritance envelopes can be appropriately applied here to

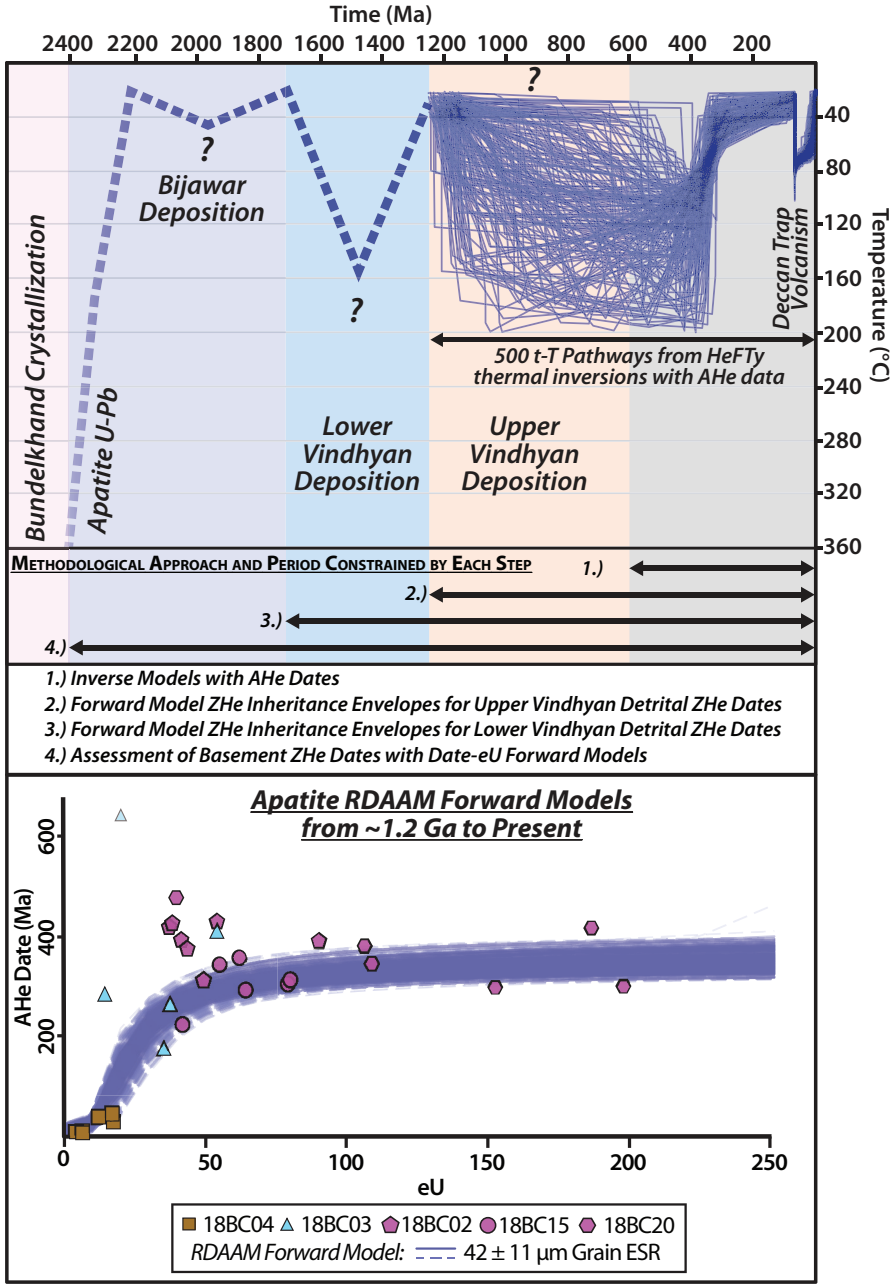

Fig. 5. Summary of known geologic constraints from central India with an outline of the methodological approach utilized to (1) extract thermal information from detrital ZHe data and AHe data, and (2) assess observed discrepancies in observed AHe and ZHe data from the Bundelkhand basement. As inverse models utilizing both ZHe and AHe inputs are cannot predict observed data for any scenario, the outlined approach was adopted using AHe inverse thermal models from Colleps and others (2021a) with detrital ZHe date-eU inheritance envelope forward models to extract meaningful thermal histories from observed data. Inverse thermal history model results using AHe data inputs from the eastern craton margin are shown as 500 individual t-T pathways from ~1200 Ma to the present, and AHe date-eU forward models for each thermal history are shown below with observed data.

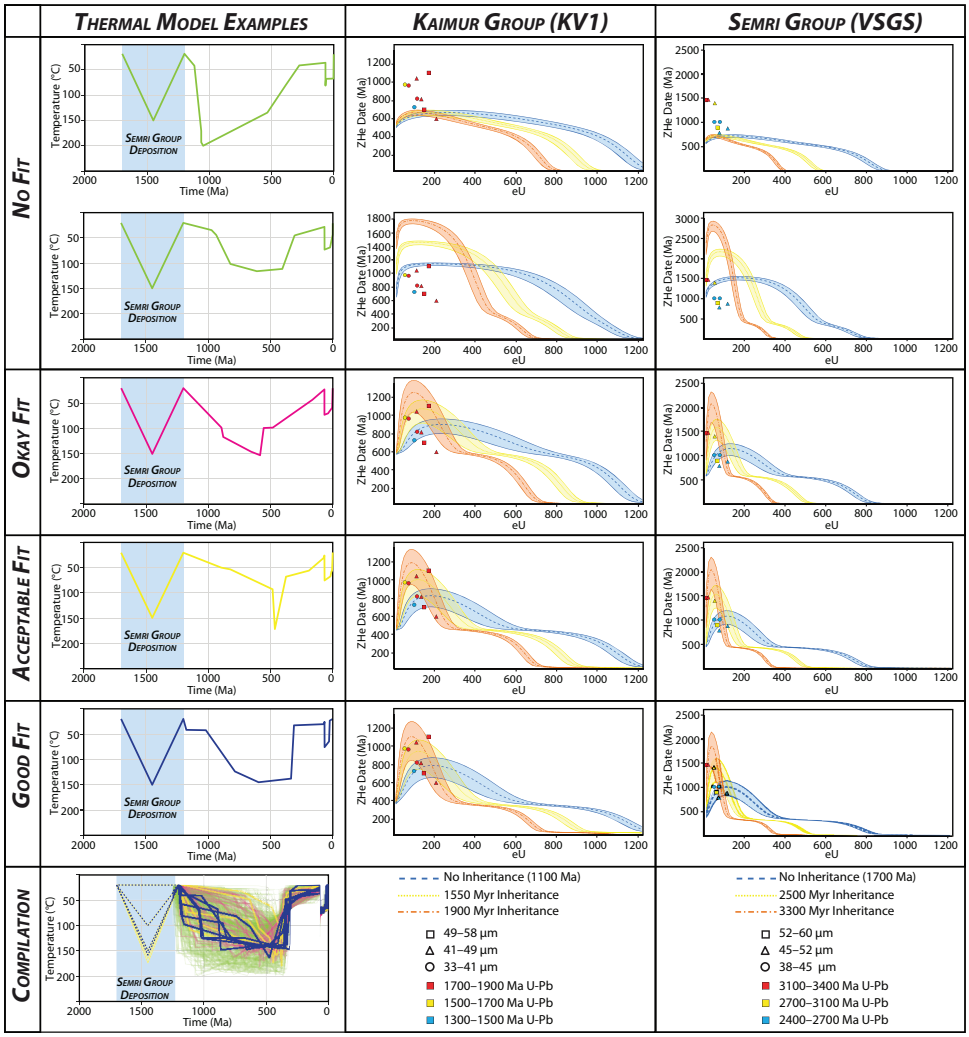

Fig. 6. Example detrital ZHe date-eU forward models showing how inheritance envelopes from the Lower and Upper Vindhyan successions were utilized to filter through t-T pathways that satisfy observed AHe data. The compilation of t-T pathways is the original result of 500 pathways that agree with observed AHe data and were simulated via AHe inverse modeling. Resulting t-T pathways were used for ZHe date-eU inheritance envelope forward models to assess their fit to observed detrital ZHe data. Date-eU inheritance envelopes were evaluated based on grain size (average ± 2 standard deviations) and U-Pb crystallization age to determine the fit of forward models to observed data. The criteria for a "good" fit require that all data points lie within a given date-eU inheritance envelope, with grain size and/or U-Pb age inconsistencies allotted for only a total of 1-2 total grains (from both Kaimur Group and Semri Group results).

constrain when and to what degree the craton experienced maximum burial temperatures since the Neoproterozoic (figs. 5 and 6).

Sampling localities along the eastern craton margin provide a unique setting to utilize this approach where basement rocks, the ~1.7–1.6 Ga Lower Vindhyan Semri Group, and the ~1.2–1.1 Ga Upper Vindhyan Kaimur Group rocks are exposed in relatively thin, condensed sections (fig. 4). The well-sampled Sangrampur hillock, for example, exposes these units within only a ~30-meter section, and it is assumed that

these rocks have experienced a near-identical low-temperature thermal evolution since the deposition of the Kaimur Group. A previous study utilized this locality to extract plausible t-T pathways from ~1.2 Ga to the present that satisfy observed AHe data, and it was shown that Deccan Traps heating thermally perturbed this location at ~66–65 Ma (Colleps and others, 2021a). Whereas derived t-T pathways from that study indicate that observed AHe date-eU results are unique to low-temperature thermal histories that require a Deccan heating event, the derived Phanerozoic and older t-T pathways remain highly scattered.

To reduce the scatter in thermal histories derived solely from AHe data, we adopted an approach that uses thermal histories from ~1.2 Ga to the present that satisfy observed AHe data (derived from HeFTy thermal inversions) and forward model date-eU inheritance envelopes to assess thermal histories that agree with U-Pb-He double dates observed from the Kaimur Group atop the Sangrampur hillock (fig. 5). Date-eU inheritance envelopes were modeled for each t-T pathway, and the goodness of fit for each envelope to observed data was assessed based on an individual grain's size and maximum helium inheritance inferred from its U-Pb crystallization age (fig. 6). Various t-T pathways were filtered out based on "no fit" (only 0–4 grains lie within appropriate envelope), "acceptable fit" (all but 2–3 grains lie within a suitable envelope), and "good fit" (all grains lie within the envelope and are concurrent based on grain size and U-Pb age) (fig. 6). After filtering, "acceptable" and "good" t-T pathways were taken and extended back to ~1.7 Ga with varying degrees of heating between 1.7 and 1.2 Ga to simulate a thermal history associated with Lower Vindhyan deposition and erosion—denoted by the major disconformity observed between the Semri and Kaimur Groups. Date-eU inheritance envelopes were forward modeled for these extended t-T pathways from ~1.7 Ga to the present, and t-T pathways were again filtered out based on fit. After final filtering, resulting t-T pathways provide thermal histories that agree with observed AHe data, Kaimur Group detrital ZHe data, and Semri Group detrital ZHe data. Lastly, t-T pathways were extrapolated back to Bundelkhand craton formation, and date-eU forward models from these histories allow to address potential reasons why ZRDAAM and RDAAM cannot be coupled to successfully reproduce observed ZHe and AHe dates across the craton via thermal inversions.

Our detrital ZHe dataset is limited to the Son Valley Vindhyan succession; in particular, results from the Semri and Kaimur groups of the Sangrampur hillock provide a unique locality with the most robust geologic constraints. Accordingly, we limit our exploration to the AHe and ZHe datasets from the eastern Bundelkhand craton margin and assume that the eastern craton experienced a uniform low-temperature thermal evolution. This assumption is supported by the fact that all basement samples were collected within an elevation difference of less than 200 meters and that the elevation of the Semri Group contact with the basement is near uniform from north-to-south across the eastern craton margin. This assumption allows for a multi-sample compilation of single-grain data to ensure a sufficient spread in AHe and ZHe date-eU space exists for meaningful long-term thermal model constraints.

AHe Inverse Models from Eastern Bundelkhand Craton Margin

To produce t-T pathways that agree with the observed AHe data from the Eastern Bundelkhand Margin for detrital ZHe assessment, we adopted an identical inverse model setup in HeFTy to that utilized by Colleps and others (2021a) (Supplementary fig. S3). However, instead of running 100,000 t-T iterations as done in Colleps and others (2021a), we set up the model to finish after 500 "good" t-T pathways were achieved (GOF: 0.5)—allowing for sufficient t-T pathways to forward model detrital ZHe date-eU inheritance envelopes and test their ability to predict observed detrital ZHe data. A total of 1,558,273 iterations were tested before 500 "good" pathways were

attained. Figure 5 shows the resulting 500 t-T pathways from ~1.2 Ga to the present, and AHe date-eU forward models for each pathway reveal how these models satisfy observed AHe data.

Detrital ZHe Date-eU Inheritance Envelopes

Kaimur Group forward models.—Following HeFTy thermal modeling to fit the AHe data, detrital ZHe date-eU inheritance envelopes were forward modelled for each of the 500 "good" t-T pathways extending from ~1250 to 1150 Ma to the present that agree with observed AHe data (figs. 5 and 6). For a zero inheritance curve, we assume a depositional age for the Kaimur Group in this locality of 1200 Ma, in accordance with maximum depositional ages of the Kaimur Group at the Sangrampur hillock derived from the youngest detrital zircon U-Pb ages (Colleps and others, 2021b) and the robust $^{40}Ar/^{39}Ar$ age of 1073.5 ± 13.7 Ma for the Majhgawan kimberlite that intrudes into the uppermost Kaimur Group (Gregory and others, 2006). For the maximum inheritance curve, we assume a maximum allotted damage and helium inheritance of 1900 Ma derived from the oldest U-Pb age of the U-Pb-He double-dated Kaimur Group suite. For each date-eU inheritance curve, a grain size window is denoted by the average Kaimur Group grain size with 2 standard deviations (45 ± 12 mm). We utilized a range from 1200 Ma (that is, zero inheritance) to 1900 Ma (that is, maximum inheritance) to model permissible date-eU envelopes to compare single grain detrital ZHe data directly. Observed ZHe dates from the Kaimur Group were assessed based on these envelopes, and the fit of these data were carefully inspected based on their grain size and U-Pb age (fig. 6). Of the 500 forward-modelled t-T pathways, 13 produced date-eU inheritance envelopes that resulted in "good" fits (as previously defined), and 37 t-T pathways produced "acceptable" fits to the observed detrital ZHe data.

Semri Group forward models.—After filtering through Kaimur Group date-eU forward models, all 13 "good-fit" t-T pathways were extended back to ~1.7 Ga to reflect the onset of Lower Vindhyan deposition (figs. 5 and 6). Whereas the extent of burial and erosion experienced by the Lower Vindhyan succession from 1.7–1.2 Ga remains uncertain, we assume a simple burial and erosional history consisting of maximum burial at ~1.45 Ga of varying magnitudes (10°; 100°; 150°; 160°; 170°; 180°C), and these simplified thermal pathways were added on to each of the previously derived "good-fit" ~1.2 Ga to present t-T pathways. Accordingly, a total of 78 extended t-T pathways from 1.7 Ga to the present were utilized to generate date-eU inheritance envelopes for assessment of the Semri Group detrital ZHe dates. Zero inheritance date-eU curves assume a depositional age of 1.7 Ga. In contrast, a maximum inheritance curve of 3.3 Ga was used based on the oldest U-Pb age from all Semri Group double-dated grains (fig. 6). Each inheritance envelope includes a grain size window of 49 ± 11 mm (average ± 2 SD).

As for Kaimur Group models, date-eU inheritance envelopes for each extended t-T pathway were compared to observed data to determine their goodness of fit. We maintained a strict filtering regime for Semri Group forward model results consistent with the Kaimur Group models and selected "good" t-T pathways based only on models that agree with all observed detrital ZHe data. As a result, only 14 of the 78 t-T pathways satisfy all observed data, and 7 of these thermal history pathways are identical from ~1.2 Ga to the present, with only the degree of Semri Group burial varying (fig. 7; Supplementary fig. S4). Importantly, this analysis further refines the range of acceptable t-T pathways from ~1.2 Ga to present, reducing the number of "good" fits within this time range from 13 to 7. In all scenarios, no t-T pathways with Semri

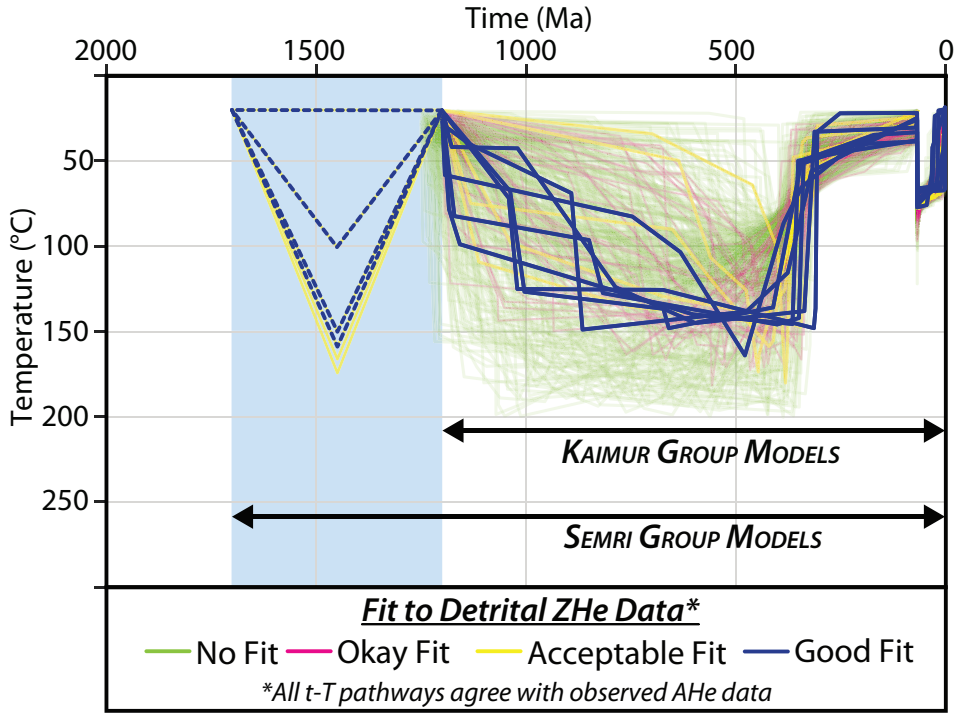

Fig. 7. Compiled summary of the results from AHe inverse thermal models and detrital ZHe forward models. The resulting "good" thermal models satisfy all detrital ZHe data and AHe data from the eastern Bundelkhand margin. These t-T pathways are utilized to assess basement ZHe data and for interpretations of the long-term thermal evolution of the Bundelkhand craton. Resulting "good" thermal histories share common similarities from ~1200 Ma to the present, including a maximum burial temperature of ~150°C between ~850 and 475 Ma, followed by a major cooling event during the late Paleozoic and a discrete Deccan reheating event.

Group burial above 160°C satisfy observed data, and most t-T pathways that satisfy observed data require broadly constrained burial temperatures of 100–160°C between 1.7 and 1.2 Ga. At this point, "good" t-T pathways agree with all detrital ZHe data from the Semri and Kaimur groups and with observed AHe dates from the eastern craton margin (fig. 7).

Bundelkhand Craton ZHe Forward Models

All t-T pathways that agree with detrital ZHe dates from Vindhyan deposits and AHe dates were extrapolated back to 2.3–2.2 Ga—the approximate timing at which the Bundelkhand craton was first exposed at the surface (Colleps and others, 2021b)—for date-eU forward models to assess observed ZHe dates directly from the craton (fig. 8). As with t-T pathways extrapolated back to Semri Group deposition, the ~2.3–1.7 Ga thermal evolution is increasingly uncertain, and two pre-Semri Group end-member scenarios were modelled with the same thermal evolution from 1.7 Ga to the present: (1) the craton was at surface temperatures from 2.3–1.7 Ga, and (2) ZHe dates were completely reset at 1.7 Ga before Semri Group deposition (fig. 8). Date-eU forward models for each t-T pathway using various annealing kinetic models (see discussion) were compared directly with samples from the eastern craton margin. However, a compilation of all craton ZHe data are included in

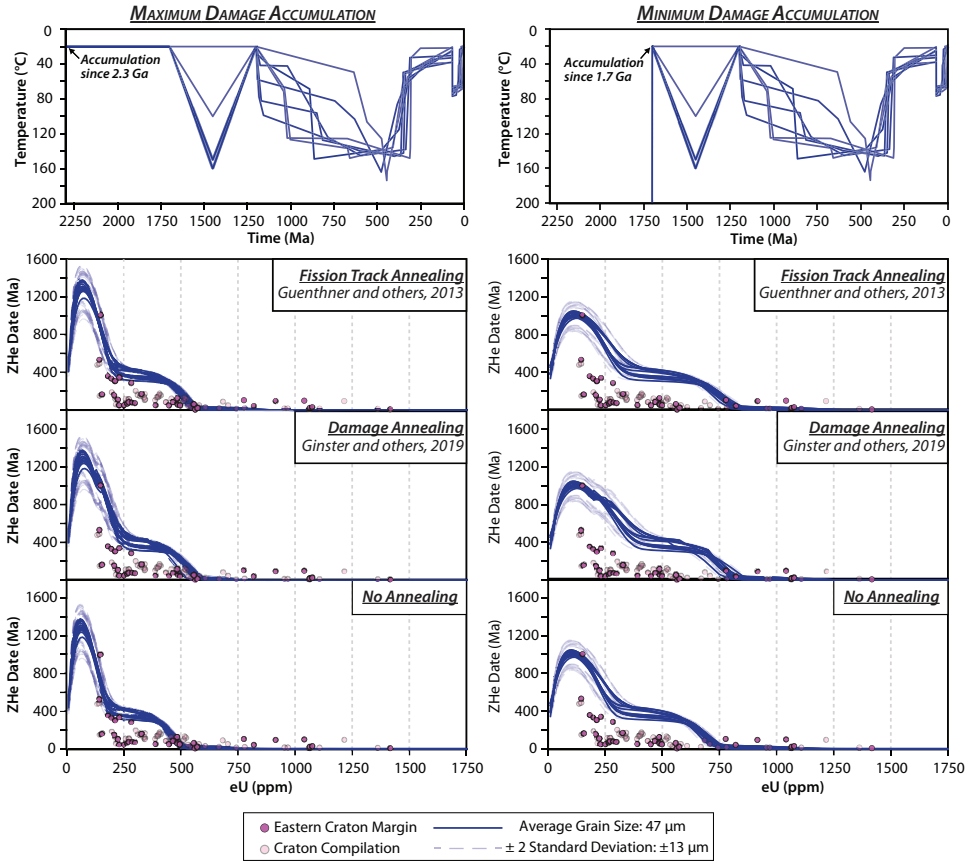

Fig. 8. Basement ZHe date-eU forward model results from previously determined "good" t-T pathways extended back to ~2.3 Ga with varying end-member scenarios, from prolonged surface temperatures before Vindhyan deposition to complete annealing and resetting at ~1.7 Ga prior to the onset of Vindhyan deposition. ZHe date-eU forward models were computed using (1) fission-track annealing kinetics of Guenthner and others (2013), (2) alpha-damage annealing kinetics of (Ginster and others, 2019), and (3) a no annealing scenario that reflects maximum end-member damage accumulation. In all scenarios, it is evident that these models overestimate ZHe dates for zircon with moderate to high levels of radiation damage (grains with eU concentrations between ~200 and 400 ppm in this case).

comparisons for reference. As expected, based on coupled AHe and ZHe thermal inversion attempts, none of the forward models could reproduce the observed date-eU trends from the craton, despite these models agreeing with detrital ZHe and AHe results (fig. 8). In all forward models, the date-eU curve is steeply negative at an eU of between 100 and 200 ppm before it flattens and forms a date-eU plateau from 200 to 400 Ma and from 200 to 600 ppm. The slope of this date-eU plateau primarily reflects the crustal cooling rate between 400 and 200 Ma in each t-T pathway—a flat plateau results from fast cooling, whereas a sloped date-eU trend reflects slow cooling (for example, Ault and others, 2018). Where this date-eU plateau occurs for each t-T pathway, ZRDAAM consistently overestimates a significant cluster of observed ZHe dates with eU values of ~200–600 ppm (fig. 8). At >600 eU, ZHe dates rapidly drop to near-zero values with exceedingly high damage, but ZRDAAM consistently underestimates observed these ZHe dates at higher eU.

DISCUSSION

The inability of coupled ZRDAAM and RDAAM kinetics to simulate t-T pathways that agree with both AHe and ZHe datasets from the Bundelkhand craton indicates that a significant discrepancy exists in one or both of these damage-dependent kinetic models. Notably, thermochronometric data across the Bundelkhand craton reveal the most extreme AHe and ZHe date inversion on record, with a ~300 Myr difference between inverted AHe and ZHe dates from grains with moderate to high damage levels (fig. 1B). Inversions in ZHe and AHe dates are expected with existing diffusion kinetics of ZRDAAM and RDAAM, as ZRDAAM predicts that exceedingly high-damage grains may exhibit ^{4}He closure temperatures (T_c) of ~50 to <0 °C (Guenthner and others, 2013), and RDAAM defines an increase in AHe T_c from ~30 to 90 °C with increasing damage (Shuster and others, 2006; Flowers and others, 2009). Although not as extreme as observed from the Bundelkhand craton, naturally occurring ZHe and AHe date inversions have been documented in several geologic settings, including the Zimbabwe Craton (Mackintosh and others, 2017) and the Colorado Front Range (Johnson and others, 2017). These studies indicate that, for thermal models that agree with AHe data, ZRDAAM tends to overestimate ZHe dates for zircon with low to moderate eU, and to underestimate ZHe dates with very high eU. Thus, the geologic conditions responsible for naturally occurring ZHe and AHe date inversions remain highly uncertain. Here, we take advantage of the unique geologic setting of central India and our unexpected ZHe and AHe results to (1) assess potential sources responsible for RDAAM and ZRDAAM discrepancies in predicting observed AHe and ZHe dates, (2) evaluate the effect of Deccan Traps volcanism on the AHe and ZHe system, and (3) utilize ZHe date-eU inheritance envelopes to extrapolate meaningful thermal information.

Potential Sources for Observed ZHe and AHe Discrepancies

For the sake of illustration and assessment, we have chosen a single t-T pathway from our inverse and forward models that most closely predicts observed basement ZHe dates as the focus of our discussion on AHe and ZHe discrepancies (fig. 9). We note that, although ZRDAAM and RDAAM adequately predict observed AHe and detrital ZHe data for this thermal history, we utilize this single t-T pathway solely as an example to assess ZRDAAM and potential sources for inconsistencies between observed data and modeled predictions. This thermal model does not definitively signify the actual thermal evolution of the craton.

Analytical uncertainties in bulk eU concentrations.—Observed date-eU discrepancies may result from inaccurate measurements of bulk U and Th concentrations in apatite and zircon. Conventional analytical procedures for U and Th measurements rely on an assumed grain mass obtained from measured grain dimensions. Assuming an idealized grain morphology, measured dimensions are used to compute grain volume, and a mass is calculated based on a mineral's density. It has recently been documented that morphometrically derived eU measurements may be inaccurate, and incorporating a ^{42}Ca and ^{90}Zr isotope dilution approach (for apatite and zircon, respectively) provides a more accurate and direct means to determine grain masses and eU concentrations (Guenthner and others, 2016). In addition, conventional microscopic dimension measurements may result in overestimates (~20–25%) for single grain masses, and eU concentrations may consequently be underestimated to a similar degree (Cooperdock and others, 2019). All U and Th measurements obtained in this study were derived from morphometric grain measurements of zircon and apatite, and these measurements may be a source of discrepancy between observed and predicted AHe and ZHe data. To account for this potential source of error to our ZHe dataset, we add a "correction" to our date-eU forward models. This correction

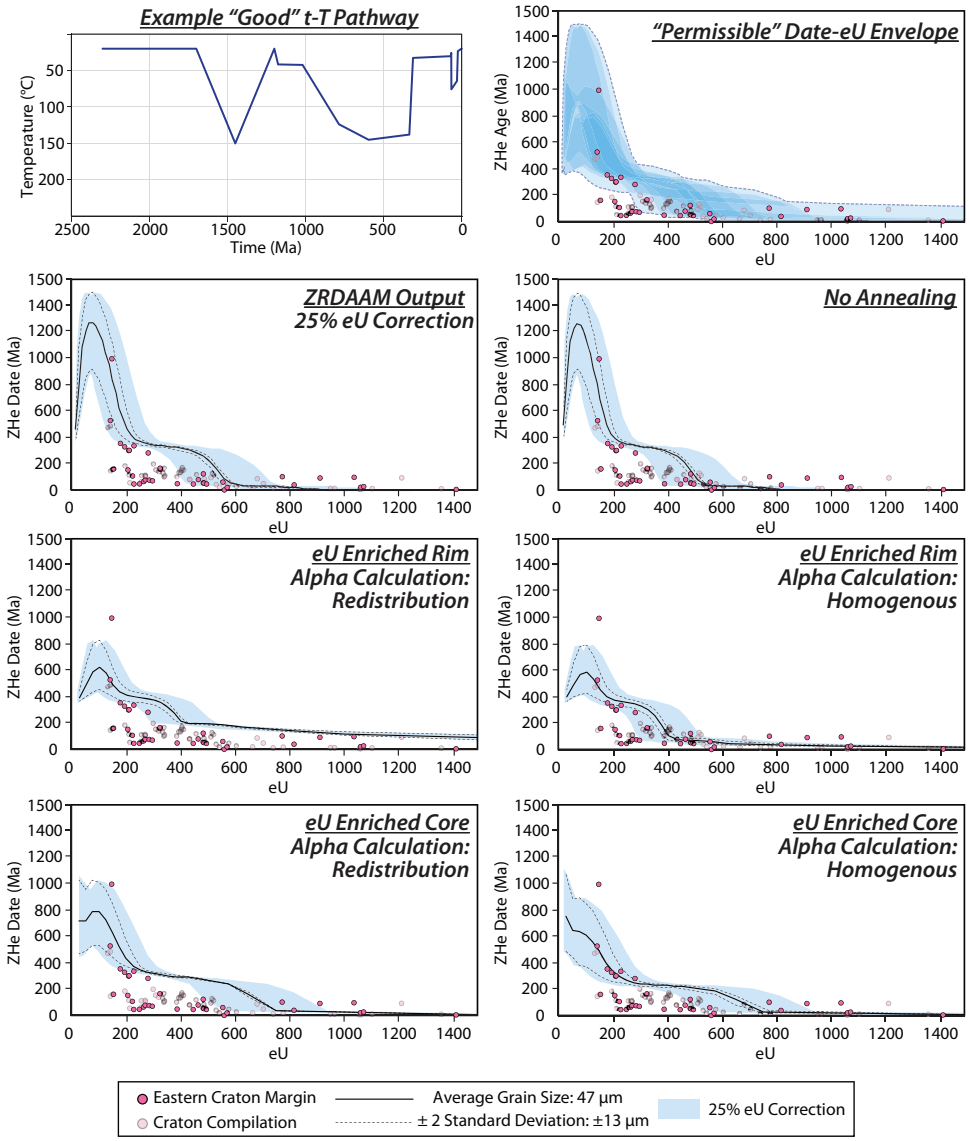

Fig. 9. Summary of various tests to assess potential discrepancies between observed and predicted ZHe data using a single t-T pathway as an example. This t-T pathway was chosen for this assessment because its resulting date-eU forward models using standard ZRDAAM parameters provided the closest fit to observed ZHe data. Date-eU forward models were simulated for end-member scenarios, including no annealing, enriched eU cores, and enriched eU rims (using both redistribution and homogeneous alpha correction factors). A 25% eU correction is applied for each scenario to account for potential sources of analytical error. All date-eU forward models were compiled to establish a "permissible" ZHe date-eU envelope. Although this "permissible" envelope satisfies significantly more data points than our standard ZRDAAM application, these models still overestimate dates from grains with eU concentrations between ~200 and 300 ppm for this given t-T pathway.

takes the previously determined average difference of 25% between the two methods for determining eU concentrations in zircon (15% average difference in apatite), and we applied this difference to date-eU forward models. For simplicity of illustration, we incorporate an isotope dilution correction envelope to date-eU forward

models where a +25% correction was applied to the largest possible grain size, and a −25% correction was applied to the smallest grain size (fig. 9). A resulting date-eU envelope indicates a broad range of date-eU that may be acceptable for the given t-T pathway. When this correction is applied to our selected t-T pathway, the date-eU envelope can predict young observed grains within eU values of ~400–600 ppm, but a cluster of grains with an eU of ~200–400 is still not accounted for (fig. 9). As this correction may be applicable in all cases, we have additionally applied this correction to forward models simulating no annealing and zonation scenarios discussed below.

Radiation damage annealing and He diffusivity.—The assumption utilized in ZRDAAM and RDAAM that radiation damage and fission tracks for each system have similar annealing kinetics may be a significant cause for discrepancy (for example, Green and Duddy, 2018). It has been well documented in zircon that complete annealing of fission tracks occurs at lower temperatures and shorter heating durations than required for complete annealing of bulk radiation damage, suggesting that existing ZRDAAM parameters may underestimate the time and temperature required for full radiation-damage annealing (Ginster and others, 2019). The potential that ZRDAAM and RDAAM overestimate the amount of damage annealing for a given t-T history may result in erroneous modelled He diffusivities.

To account for this potential discrepancy to our dataset, we assess how an end-member scenario in which zircon experienced no damage annealing may impact observed ZHe dates. We compare these predictions directly to ZHe date-eU forward models using the ZRDAAM kinetics of Guenthner and others (2013) (based on fission-track annealing) and Ginster and others (2019) (based on alpha-damage annealing) (figs. 8 and 9). Predicting date-eU trends based on a diffusivity model that ignores annealing allows diffusivities to be derived from an end-member scenario where the maximum possible damage accumulation is achieved for a given t-T pathway. Compared to the ZHe date-eU forward models derived using up-to-date fission-track and alpha-damage annealing kinetics, the shape of the date-eU curve with annealing turned off remains similar, but the curve is shifted to lower eU values (figs. 8 and 9). This shift signifies that grains with moderate eU values likely accumulated more damage than ZRDAAM predicts, and thus the diffusivities of these grains for the given thermal history are greater.

In ignoring annealing, the resulting date-eU forward model more adequately predicts observed ZHe dates between eU values of 200 and 600 ppm, although a significant discrepancy between predicted and observed data still exists (fig. 9). Whereas an overestimate for damage annealing is likely a major contributor to the observed disparities between ZRDAAM-predicted and observed ZHe dates, end-member forward models still do not entirely agree with observed data, and additional factors are likely at play. In addition, the damage-annealing kinetics for the apatite system remains uncertain, and RDAAM may also overestimate damage annealing (for example, Fox and Shuster, 2014; Willett and others, 2017). If damage annealing is overestimated in both ZRDAAM and RDAAM, it is not surprising that these models cannot adequately predict naturally occurring ZHe and AHe date inversions, particularly in geologic settings, like central India, that have experienced a prolonged history at low temperatures. If damage annealing is overestimated, ZRDAAM may underestimate zircon diffusivity with low to moderate eU, whereas RDAAM may overestimate diffusivities in low to moderate eU apatite grains. It is worth noting here that the damage-induced percolation transition—the point at which He retentivity decreases—may also occur at alpha doses lower than those utilized in ZRDAAM (Anderson and others, 2017; Gautheron and others, 2020). Diffusivities for highly damaged zircon may also be underestimated, as recent studies have shown that heavily damaged zircon may even yield closure temperatures lower than average surface temperatures (Cherniak,

2019). Uncertainty in modeling damage accumulation over time, coupled with the overestimated percolation transition zone, will only amplify disparities in observed and modeled data. The complex nature of the accumulation of multiple types of radioactively-induced lattice defects—each with their unique annealing kinetics—additionally exacerbates such uncertainties. Thus, an increased understanding of damage-accumulation and annealing kinetics for apatite and zircon is required to refine diffusion models, and we note that this is well beyond the scope of this study.

Impact of U and Th zonation.—Zonation of uranium and thorium can significantly impact the AHe and ZHe systems (for example, Farley and others, 2011; Ault and Flowers, 2012; Gautheron and others, 2012; Murray and others, 2014; Peak and others, 2021), although it remains unclear how nonhomogeneous damage accumulation resulting from concentrated uranium and thorium clusters may impact ^{4}He diffusivities over prolonged periods. Detailed Raman mapping of α-dose in ancient zoned zircon confirms complex intracrystalline variations in radiation damage that may result in significant data dispersion (Anderson and others, 2020). Unfortunately, we do not have predetermined U and Th zonation information for grains selected for ZHe analysis. In the absence of direct zonation measurements, we employed a forward modeling exercise that accounts for extreme end-member representations of eU zonation. This approach provides a valuable indirect assessment on the potential impact of zonation on ZHe date-eU dispersion within a given dataset.

If a grain exhibits eU zonation, a homogenous alpha ejection correction factor will result in an He date that is too young if eU is preferentially concentrated in its rim, or too old if its core has a higher eU concentration (Farley and others, 1996; Hourigan and others, 2005). Accordingly, a zoned alpha ejection correction can be applied to account for He redistribution. Both ejection corrections are incorporated into HeFTy and computed based on input U and Th zonation profiles. Here, we utilize the forward modeling capabilities in HeFTy to test the He date-disparity impact of two end-member zonation scenarios applied to our example t-T pathway (fig. 9). We take the approach of Guenthner and others (2013) and use a zonation impact index defined as the whole grain eU concentration divided by the concentration difference between the core and the rim. We assume a worst-case scenario for each date-eU relationship and select end-member zonation profiles that maximize the difference in damage-induced diffusion kinetics between the core and rim. To maintain a maximum zonation impact index, we selected core eU values that differ from a grain's bulk eU concentration by a factor of seven (Guenthner and others, 2013). We select a core radial position that is 1/3 of the grain radius from the center for enriched core zircons, and 2/3 from the center for enriched rim zircons. As a result, the ratio of eU concentrations between the rim and core is 9.52:1 for enriched rims and 1:9.1 for zircons with enriched cores (Guenthner and others, 2013).

We model date-eU curves for such extremely zoned grains with a range of grain sizes (craton average ± 2 SD) and our selected t-T pathway for comparison, and predicted data using both a homogenous and a redistributed alpha correction are reported (fig. 9). The resulting date-eU forward models for zircons with highly enriched eU cores provide younger dates for grains with low eU, and a significantly longer plateau between 200 and 400 Ma at moderate to high eU. At high bulk eU concentrations, dates rapidly drop to less than ~30 Ma. Forward models for zircon with enriched eU rims show a similar decrease in ZHe dates at low bulk eU concentrations but result in a subtler 200–400 Ma plateau at low to moderate bulk eU concentrations. Interestingly, a second date-eU plateau forms at bulk eU concentrations >400 ppm with significantly older ZHe dates than for unzoned or enriched core zircons. At bulk eU values between ~500 and 1500 ppm, modeled ZHe dates gradually ZHe date decrease from ~200 Ma to ~80 Ma (fig. 9). Older ZHe dates at high bulk eU concentrations in zircon with

highly enriched eU rims are likely the result of trapped He within low eU cores, which likely amassed a low to moderate amount of damage accumulation—a core with low diffusivities surrounded by a domain of high damage and high diffusivities in the rim.

Whereas highly enriched eU rims show promise to adequately explain observed ZHe dates with high bulk eU concentrations, forward model results for zircons with either enriched eU cores or rims cannot reproduce observed ZHe dates at moderate eU concentrations between ~200 and 600 ppm (fig. 9). It is important to emphasize that these scenarios assume perhaps the most extreme zonation end-member examples. If predicted ZHe dates from heavily zoned grains are still discordant from observed data in even end-member scenarios, other factors likely contribute to these disparities.

Compilation of potential sources of discrepancies.—In figure 9 we have compiled all date-eU forward models that account for the potential impacts of zonation, differing annealing kinetics, and analytical errors on data dispersion for our example t-T pathway. We illustrate a broad range of date-eU predictions that may be deemed a permissible envelope for comparison to observed data. However, even with this generous envelope that accounts for rather extreme scenarios, these models are still not capable of adequately predicting young ZHe dates with low to moderate bulk eU concentrations. Although we provide a single example for a given thermal history, the observed shifts in date-eU curves are fairly systematic for each t-T pathway that agrees with AHe and detrital ZHe data. Our chosen t-T pathway yields a date-eU curve that most closely fits observed data. If the permissible date-eU envelope for this t-T pathways cannot predict the observed data from this thermal history, then it is justifiable to expect that the remaining "good" t-T pathways will not agree with this systematic shift either.

This example illustrates the inherent complexities of the ZHe system that may lead to extreme ZHe date disparities and illustrates how imperative it is to avoid ambiguities presented in the use of conventional (U-Th)/He analytical methods for long-term thermal modeling. Tracking zonation of U and Th via laser ablation ICP-MS analyses (for example, Peak and others, 2021) and measuring eU based on the Ca and Zr isotope dilution procedure of Guenthner and others (2016) can be quickly adopted to reduce these uncertainties. In addition, uncertainties associated with conventional microscope grain dimension measurements may also be lessened by utilizing 3D x-ray computed tomography for precise measurements (Cooperdock and others, 2019).

The same complexities illustrated above for the ZHe system likely exist in the AHe system. It may very well be the case that tested t-T pathways that agree with AHe and detrital ZHe data (derived using standard ZRDAAM and RDAAM parameters) are erroneous, as the same effects of annealing and zonation illustrated above were not accounted for and may significantly impact resulting t-T pathways. However, we argue that, for reasons previously discussed, these t-T pathways provide important temporal and thermal constraints for the Bundelkhand region. It remains highly uncertain what exactly is causing the major disparity in observed and predicted basement ZHe dates, but we consider that Deccan Traps volcanism likely had a drastic impact on observed thermochronometric data that current diffusion models cannot predict, as discussed below.

Impact of Deccan Traps Volcanism on AHe and ZHe Dates

We speculate that ZRDAAM and RDAAM are not sufficiently calibrated to be coupled in predicting a rapid heat pulse that occurred in a late phase relative to a prolonged period at low temperatures; such is the case with the Deccan Traps LIP in central India. Thermal inversions using RDAAM parameters require a late heat pulse to satisfy observed AHe data, most probably linked to a Deccan Traps-induced reheating event via either (1) burial beneath thick basaltic flows, (2) top-to-bottom conductive heating from hot lava flows, or (3) a temporary increase in regional heat flux (see Colleps and others (2021a) for further discussion). However, it is unclear how such

an event may affect the ZHe system, especially when zircons are likely to have experienced a prolonged complex history of damage accumulation and annealing. It has been previously suggested that LIP magmatism has the potential to overprint damaged ZHe dates—thermal models utilizing ZRDAAM and RDAAM from the South American passive margin record a plausible reheating event that may be associated with the Early Cretaceous Paraná LIP (Hueck and others, 2018). However, unlike in central India, AHe dates from the South American passive margin were completely reset after LIP magmatism. Based on the AHe thermal inversions for central India of Colleps and others (2021a) utilized in this study, Deccan Traps volcanism only partially reset apatite with low eU concentrations, whereas high eU AHe dates significantly pre-date Deccan Traps magmatism. In contrast, most zircon with high eU concentrations yield ZHe dates that post-date Deccan Traps volcanism. In particular, compiled zircon from the eastern Bundelkhand margin with eU concentrations >400 ppm yield an average ZHe date of ~58 Ma—only ~7–8 Myrs younger than Deccan Traps volcanism (Schoene and others, 2015; Sprain and others, 2019). The resulting >300 Myr date inversion between AHe and ZHe dates may be the result of Deccan Traps volcanism, and RDAAM and ZRDAAM may not be calibrated to adequately account for the duration and magnitude of such an event at the resolution necessary to predict naturally occurring kinetic crossovers in He diffusivities between the AHe and ZHe system (Reiners, 2009).

To assess differing impacts of Deccan Traps volcanism on ZRDAAM and RDAAM date-eU predictions, we modify our example t-T pathway to simulate Deccan Traps heating at varying magnitudes up to 180°C (fig. 10). Interestingly, the date-eU curve between eU values of ~200 and 500 ppm is predominantly affected by the magnitude of this heating. Increasing the maximum temperature of Deccan Traps heating results in date-eU curves that gradually agree with all observed ZHe dates from the craton (fig. 10). However, as expected, increasing the heating to magnitudes >75°C results in AHe date-eU forward models that depart from observed AHe data. Particularly important is that when increasing the magnitude of Deccan Traps heating up to 180°C, the ZHe date-eU curve remains relatively unchanged at an eU of between 0 and 200 ppm (fig. 10). Whereas t-T pathways derived from detrital ZHe dates rely heavily on the date-eU curve from 0-200 ppm eU, these adjustments to the magnitude of Deccan Traps heating up to 180°C do not significantly affect the goodness of fit of observed data to resulting inheritance envelopes (fig. 11). This portion of the date-eU trend is primarily controlled by the timing and magnitude of Proterozoic–Early Paleozoic heating.

This simulation illustrates that relatively minor shifts in the magnitude of Deccan Traps heating can impact the predicted ZHe and AHe dates from grains with moderate to high damage accumulations (figs. 10 and 11). Given that the closure temperature range of high-damage apatite is unlikely to exceed 110°C, it may be the case that ZRDAAM currently overestimates ZHe dates of zircon grains with eU concentrations between 200 and 600 ppm in this scenario. Accordingly, if observed ZHe and AHe discrepancies are due to model calibration issues, it is likely the case that ZRDAAM calibrations need to be refined as opposed to RDAAM. Refinement of these models to adequately record such short-lived and late-phased heat pulses have the potential for improving the robustness of long-term low-temperature thermal models.

Thermal Evolution Derived from Detrital ZHe Forward Models

Despite the inability of coupled ZRDAAM and RDAAM inverse models to adequately predict observed AHe and ZHe data from the Bundelkhand craton (for reasons discussed above), we argue that meaningful long-term thermal models can still be derived from central India in our approach by using detrital zircon date-eU

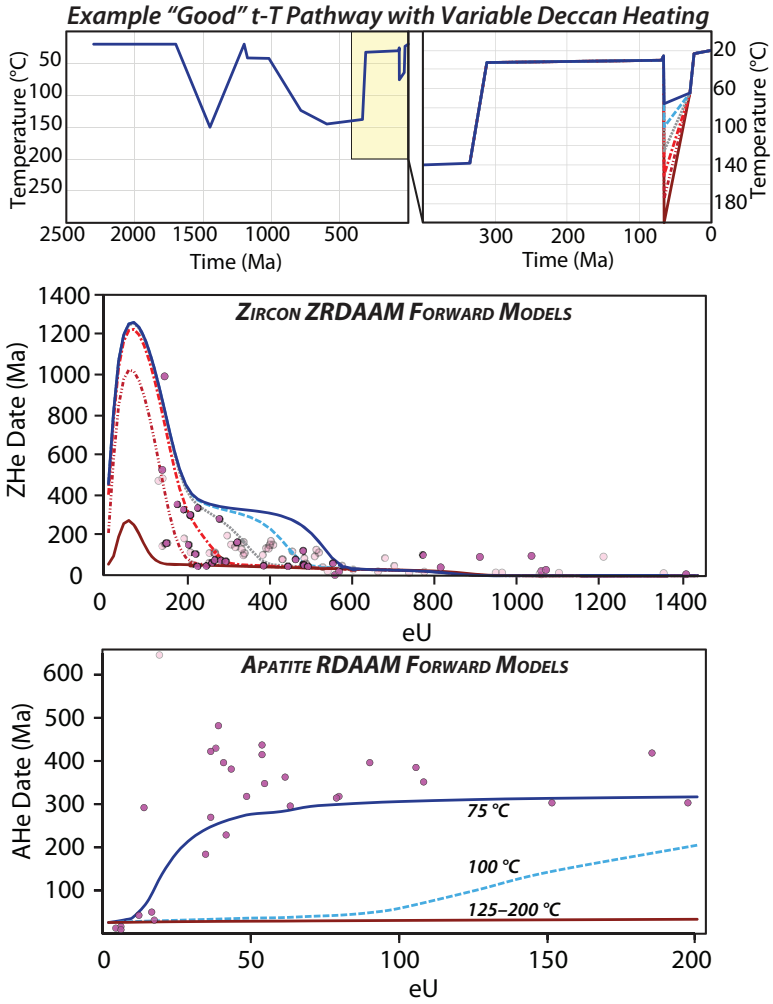

Fig. 10. Forward model results showing the impact a heat pulse of varying magnitudes related to Deccan Traps emplacement may have on ZHe and AHe date-eU curves using standard RDAAM and ZRDAAM parameters. Increasing the magnitude of Deccan Traps heating from ~100–180°C results in ZHe date-eU curves that satisfy observed ZHe data, but observed AHe data cannot be reproduced for heating magnitudes above ~75°C.

inheritance envelopes. This approach produces 14 robust t-T pathways (from a total of 1,558,273 originally tested pathways) that agree with observed detrital ZHe data from the Lower and Upper Vindhyan deposits and AHe data from the eastern Bundelkhand craton margin (figs. 6 and 7). Although this approach relies on ZRDAAM forward models, we highlight that (1) the majority of observed model discrepancies occur within a limited range of eU concentrations (~200–600 ppm), accounting for moderate- to high-damaged basement zircon, and (2) older cratonic ZHe dates from low eU grains (<200 ppm) are consistently predicted by the models (fig. 8). All detrital ZHe grains yielded anomalously low eU concentrations, and we demonstrate above that this portion of date-eU forward models is only minimally affected by the various potential sources of data disparities. Accordingly, it is reasonable to assume that, despite the observed limitations of damage-dependent diffusion models, ZRDAAM is sufficiently calibrated

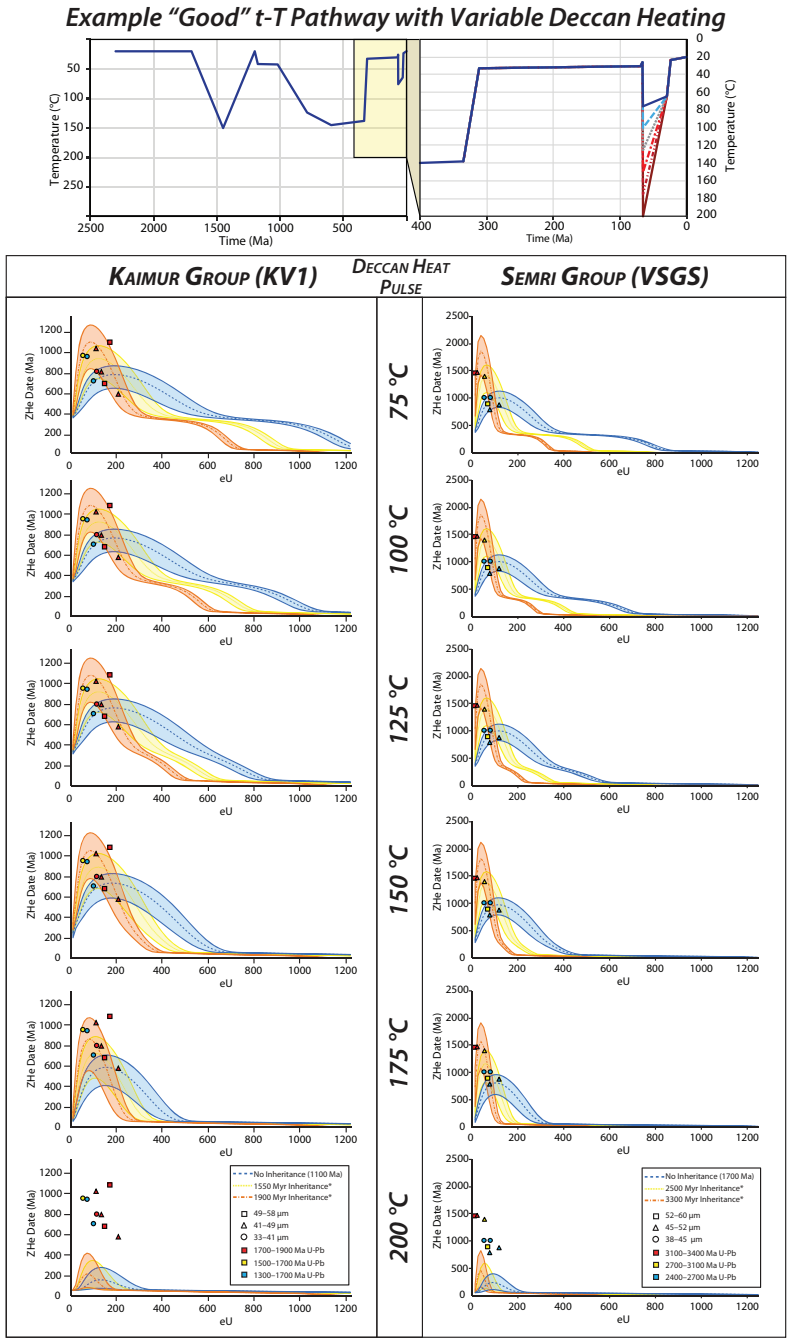

Fig. 11. Detrital ZHe date-eU forward models showing how Deccan Traps heating of various magnitudes may impact resulting inheritance envelopes used to determine plausible thermal histories. Importantly, the date-eU curve within the eU range of observed detrital ZHe data remains relatively constant for Deccan Traps heating magnitudes up to ~175°C. This result indicates that the date-eU curve within the eU range of observed detrital ZHe data is only sensitive to the older thermal evolution. Extended t-T pathways extracted from detrital ZHe data are suitable for interpreting the long-term thermal evolution of central India.

to predict ZHe dates within the observed range of eU concentrations of analyzed detrital grains. This finding is further supported by the comparatively robust empirical constraints on ^{4}He diffusivities in low-damaged zircon (that is, low-eU detrital zircon observed here) compared to high-damaged zircon. The preferential preservation of low-eU detrital apatite and zircon observed within the Vindhyan deposits may reflect the destruction of high-damage grains during sediment transport (Dröllner and others, 2022). If true, targeting old clastic rocks within cratonic settings for (U-Th)/He analyses could increase the probability of extracting apatite and zircon with low eU concentrations, which may, as demonstrated here, preserve important thermal information.

Vindhyan burial.—With this assumption in place, we can begin to interpret our compilation of t-T pathways that agree with all observed detrital ZHe and AHe data. We primarily focus on the thermal history from ~1.2 Ga to the present, which provides the most robust thermal models that agree with detrital ZHe dates from the ~1.7 Ga Semri Group. Thermal models that incorporate a ~1.7–1.2 Ga burial and erosion history of the Semri Group indicate that nearly all t-T pathways from 1.2 Ga to the present require maximum burial of ~150–160°C for date-eU inheritance envelopes to agree with observed ZHe dates from the Semri Group (fig. 7). However, the resolution of the Semri Group thermal history remains low, with plausible peak ~1.7–1.2 Ga burial temperatures ranging between 20 and 160°C. As a result, it is challenging to interpret the highly variable ~1.7–1.2 thermal evolution, and inheritance envelopes applied to the Semri Group were primarily utilized to constrain the 1.2 Ga to present thermal evolution.

Focusing on the thermal history since Kaimur deposition (~1.2 Ga) to the present, compiled t-T pathways indicate that the eastern Bundelkhand craton margin experienced average peak burial temperatures of ~150°C broadly between 850 and 475 Ma (fig. 7). Most t-T pathways indicate that the most prominent phase of heating occurred by ~850 Ma—consistent with known depositional ages of the uppermost Upper Vindhyan succession (Malone and others, 2008; Gopalan and others, 2013; Turner and others, 2014). Assuming a range of geothermal gradients between 20 and 30°C/km during the Proterozoic and an average surface temperature of 25°C, maximum burial temperatures correspond to burial depths of ~4.2–6.3 km for the Upper Vindhyan succession. The subsidence mechanism for Upper Vindhyan deposition remains debated, as interpretations that the Upper Vindhyan succession reflects deposits within an intracratonic sag basin (Bose and others, 2001; Sarkar and others, 2002; Bose and others, 2015) drastically differ from interpretations that they represent an ancient foreland basin system (Mishra, 2011; Meert and Pandit, 2014; Mishra, 2015; Shukla and others, 2019). Unfortunately, the resolution of plausible Upper Vindhyan burial histories extracted from our thermal models is insufficient to resolve these disputed subsidence mechanisms.

Late Paleozoic cooling and Deccan reheating.—All t-T pathways indicate a major cooling phase from ~150°C to ~50°C that initiated between ~450 and 350 Ma and finished between 350 and 310 Ma (fig.7). This phase of cooling is additionally apparent at a low-resolution in the compilation of 500 t-T pathways resulting from the AHe thermal history inversions (fig. 5), suggesting that such an event was required to satisfy the observed AHe dataset. We suggest that this late-Paleozoic cooling phase reflects the denudation of the craton and surrounding Proterozoic basins on the order of ~3.3–5.0 km. Notably, this erosive event post-dates Cryogenian Snowball Earth glaciations, which have been proposed as drivers of major erosion across the globe and responsible for the formation of the Great Unconformity (Keller and others, 2019; McDannell and others, 2022). If the Cryogenian Snowball Earth event did increase erosion within continental interiors at the global scale, it would be expected that ZHe and AHe data from Bundelkhand craton would record this event. However, our thermal models

indicate that crustal cooling initiated much later in central India, suggesting that the extent of glacial erosion associated with Snowball Earth may have only been limited to certain regions. Alternatively, evidence for major diachronous erosional events within continental interiors at the global-scale may allude to diachronous development of Great Unconformity erosional surfaces at the continental-scale (for example, Flowers and others, 2020; Peak and others, 2021). The absence of Neoproterozoic erosion in central India also suggests that the Bundelkhand region was not an erosional source for Cryogenian diamictite deposits along the north Indian margin, now preserved within the Lesser Himalaya of northwest India (McKenzie and others, 2011; Colleps and others, 2018).

To pinpoint potential driving mechanisms for this late-Paleozoic pulse of crustal cooling in central India, we consider the tectonic, paleogeographic, and climatic setting of central India. First, we note that this cooling event post-dates Pan-African amalgamation (Stern, 1994), that central India was part of the interior of Gondwana and far away from tectonic boundaries (Meert, 2003), and that no deformation of this age is reported from central India. Thus, it is unlikely that late-Paleozoic crustal cooling in central India directly resulted from regional tectonic uplift. Instead, late Paleozoic crustal cooling was likely the result of epeirorogenic uplift and/or climatically enhanced denudation.

It is possible that late Paleozoic erosion was epeirorogenically controlled, with dynamic topographic uplift resulting from either (1) mantle upwelling associated with indirect, far-away marginal tectonism (for example, DeLucia and others, 2017), (2) the central Indian continent drifting over a mantle plume (for example, Zhang and others, 2012), and/or (3) late continental emergence of central India associated with the gradual increase in continental elevations due to the buoyancy contrast between the crust and a cooling mantle over time (Lee and others, 2018). Whereas we can only speculate on the possibility of the latter two causes, we consider the broader tectonic evolution of Gondwana during this time to assess the potential impact of tectonics at the plate margins may have on the continental interior of India. Perhaps the most significant tectonic events with a potential temporal and spatial relationship to Bundelkhand exhumation were two independent extensional events along the northern Gondwana margin during the Early Devonian and late Carboniferous (Pennsylvanian) linked to the formation of the Asian Hun terrane and the Cimmerian terrane, respectively (Stampfli and Borel, 2002; Blakey and others, 2008). However, we note that these extensional events were >2000–3000 km north of the Bundelkhand region and resulted in the formation of only narrow, ribbon-like terranes stripped off the northern Gondwanan margin. In addition, the onset of the Early Devonian formation of the Asian Hun terrane pre-dates the major ~350–310 Ma pulse of crustal cooling in central India, and the Pennsylvanian formation of the Cimmerian terrane postdates the onset of this event. Accordingly, we consider it unlikely that the formation of these narrow terranes would have resulted in epeirogenic uplift of the Bundelkhand region. Although epeirogenic uplift linked to far-away tectonic processes has been attributed to phases of erosion within the continental interior of the United States (for example, DeLucia and others, 2017), we note that these phases coincide with supercontinent-scale extensional events associated with the breakup of much larger terranes.

Alternatively, it is possible late Paleozoic erosion in central India was climatically induced. During this period, India was positioned at high latitudes alongside a broad area of Gondwana, including Antarctica and Australia (Stampfli and Borel, 2002; Blakey and others, 2008) (fig. 12). Interestingly, the onset of ~350–310 Ma erosion in central India coincides with the onset of the late-Paleozoic icehouse, the longest-lived glacial period of the Phanerozoic (Montañez and Poulsen, 2013). This temporal coincidence suggests that crustal cooling in central India could have been driven by glacial erosion

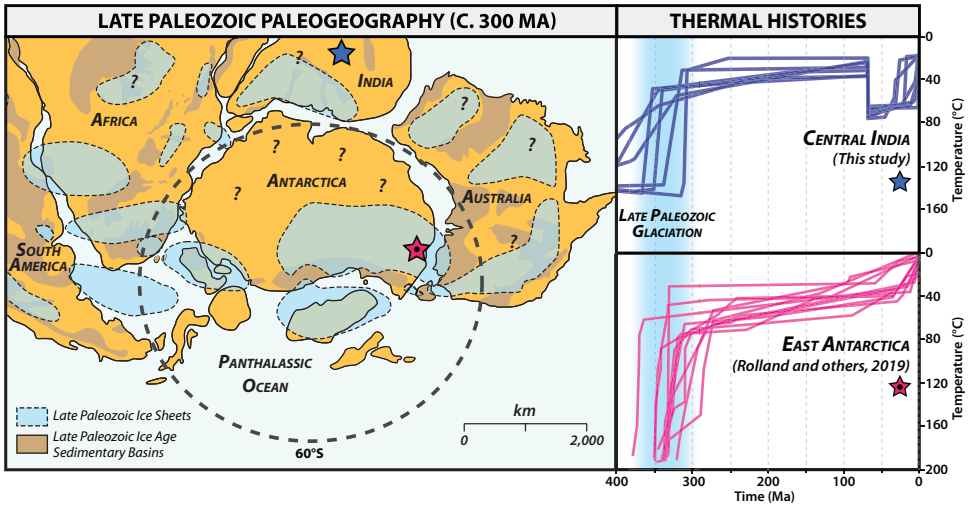

Fig. 12. Late Paleozoic paleogeographic reconstruction with previously speculated extents of late Paleozoic ice sheets and sedimentary basins. Low-temperature thermal history models from central India (blue star; this study) and east Antarctica (pink star; Rolland and others, 2019) share a common pulse of late-Paleozoic cooling potentially linked to enhanced glacial erosion during the late-Paleozoic ice age. Paleogeographic map with ice extent modified from Montañez and Poulsen (2013) and (Isbell and others, 2012).

linked to the southern hemisphere icesheet during the late Paleozoic. Recent low-temperature thermochronometric data from East Antarctica reveal a very similar pulse of crustal cooling between ~340 and 300 Ma along a 600 km transect, which was proposed to reflect significant erosion by temperate glaciers during the late-Paleozoic ice age (Rolland and others, 2019) (fig. 12). Late-Paleozoic thermal models from Antarctica are remarkably similar to those observed in central India, providing evidence that two separate continents at near-polar latitudes during the late-Paleozoic ice age experienced a coeval pulse of erosion at similar magnitudes from ~350–310 Ma. Given their paleogeographic proximity, it is reasonable to assume that a shared mechanism drove ~350–310 Ma erosion within India and Antarctica. As suggested for central India, thermal models in Antarctica are inconsistent with exhumation linked to Permian rifting (Rolland and others, 2019). Furthermore, Early Permian glacial-marine deposits of peri-Gondwanan origin have been discovered within the India-Asia collision zone of Northern Ladakh, which is believed to have split from the northern Gondwana margin as part of the Cimmerian microcontinent (Upadhyay and others, 2022); these sediments may have been sourced from central India. Accordingly, we find glacial scouring during the late Paleozoic ice age the most convincing driver for the ~350–300 Ma phase of crustal cooling observed in central India.

Following this significant pulse of late-Paleozoic erosion, thermal models indicate that the craton was slowly denuded to near the surface by 66 Ma, when a heat pulse that we relate to the Deccan Traps may have overprinted the AHe and ZHe systems, and basaltic flows were emplaced above Vindhyan strata at varying stratigraphic horizons (fig. 7). If RDAAM adequately models the extent of Deccan Traps heating based on observed AHe data, then thermal models indicate an average Deccan Traps heat pulse magnitude of ~72°C. If this heat pulse results from burial heating by basaltic lava flows, this temperature corresponds to a thickness of ~1.6 km, assuming a heightened geothermal gradient of 30°C/km and an average surface temperature of 25°C (Colleps and others, 2021a). Thermal models indicate a pulse of Cenozoic cooling following

Deccan Traps heating. If the Deccan Traps heat pulse is reflective of basaltic burial up to ~1.6 km, Cenozoic cooling may result from exhumation linked to uplift along the Himalayan foreland basin forebulge. However, although reheating due to burial beneath thick basaltic packages is plausible, the exact mechanism for this observed thermal perturbation remains unclear and requires additional detailed assessment (for example, Colleps and others, 2021a).

CONCLUSION

This study presents new low-temperature thermochronometric data from the Bundelkhand craton that reveal an extreme radiation-damage induced thermochronometric date inversion of over 300 Myrs between the AHe and ZHe systems. The inability for thermal-history inversions incorporating ZRDAAM and RDAAM parameters to establish t-T pathways that adequately fit with observed ZHe and AHe data from the craton indicates inconsistencies in current radiation damage-dependent kinetic models for He diffusion. Whereas the impacts of U and Th zonation, analytical uncertainties in eU concentrations, and an incomplete understanding of damage annealing kinetics likely contribute to data dispersion, we demonstrate that these factors alone cannot fully account for the discrepancy between observed and predicted ZHe and AHe data. We consider that current diffusion models are not adequately calibrated at the resolution necessary to predict a short-lived heat pulse that occurred in a late phase relative to a prolonged period of extensive damage accumulation, as is the case in central India with heating resulting from Deccan Traps emplacement overprinting AHe and ZHe dates.

Despite the inability to utilize inverse thermal history modeling with coupled basement ZHe and AHe datasets, meaningful thermal histories were extracted from detrital ZHe data with anomalously low eU concentrations and notably older ZHe dates, which preserve imperative thermal information otherwise lost in the basement record. The application of detrital ZHe date-eU inheritance envelopes provides t-T pathways that agree with all observed detrital ZHe data and AHe data from the Bundelkhand region. The resulting thermal models indicate that the Bundelkhand craton and surrounding Proterozoic basins have spent much of their existence at relatively low temperatures. The craton last experienced peak burial to temperatures of ~150°C (~4.2–6.3 km) broadly between 850 and 475 Ma. Following burial associated with Upper Vindhyan deposition, the craton likely experienced a period of stasis, followed by a glacially driven erosional event between ~350 and 310 Ma, when India was at high southern latitudes. This event can be correlated with a similar proposed pulse of erosion recorded in Antarctica, which was relatively close to India during the late Paleozoic. The craton and Vindhyan successions were cooled to near-surface temperatures by 66 Ma, followed by a heat pulse that we link to emplacement of the Deccan Traps and that may have overprinted ZHe dates in zircons with moderate to high levels of damage accumulation.

Although this study reveals significant inconsistencies in the application of current radiation-damage impacted diffusion models to unique geologic settings such as central India, we provide unique insight into observed discrepancies that may guide the empirical refinement of these models. Refining these kinetic models to predict short-lived thermal perturbations, such as LIP magmatism, is critical to improving the robustness of thermal models for interpretation, especially as researchers increasingly seek to extract prolonged low-temperature thermal evolutions from geologic settings across the globe.

ACKNOWLEDGMENTS

This work was supported by funds to NRM by the Hong Kong Research Grants Council Early Career Scheme (RGC-ECS-27305417), and by a University of Hong Kong Postgraduate Scholarship and a Hung Hing Ying Scholarship to CLC. We thank Devon Orme, Matthew Fox, and Editor Mark Brandon for their insightful reviews and feedback, which helped to improve this manuscript. We are grateful for the analytical support of Rudra Chatterjee and Des Patterson. All zircon and apatite (U-Th)/He data with sample details are provided in the supplementary material.

SUPPLEMENTARY DATA

https://earth.eps.yale.edu/~ajs/SupplementaryData/2022/Colleps/

REFERENCES

Adnan, A., and Shukla, U. K., 2014, A case of normal regression with sea level transgression: Example from the Ganurgarh shale, Vindhyan basin, Maihar area, M.P., India: Journal of the Geological Society of India, v. 84, n. 4, p. 406–416, https://doi.org/10.1007/s12594-014-0146-7

Anderson, A. J., Hodges, K. V., and van Soest, M. C., 2017, Empirical constraints on the effects of radiation damage on helium diffusion in zircon: Geochimica et Cosmochimica Acta, v.218, p.308–322, https://doi.org/10.1016/j.gca.2017.09.006

Anderson, A. J., Hanchar, J. M., Hodges, K. V., and van Soest, M. C., 2020, Mapping radiation damage zoning in zircon using Raman spectroscopy: Implications for zircon chronology: Chemical Geology, v. 538, p. 119494, https://doi.org/10.1016/j.chemgeo.2020.119494

Ault, A. K., and Flowers, R. M., 2012, Is apatite U–Th zonation information necessary for accurate interpretation of apatite (U–Th)/He thermochronometry data?: Geochimica et Cosmochimica Acta, v. 79, p. 60–78, https://doi.org/10.1016/j.gca.2011.11.037

Ault, A. K., Flowers, R. M., and Bowring, S. A., 2013, Phanerozoic surface history of the Slave craton: Tectonics, v. 32, n. 5, p. 1066–1083, https://doi.org/10.1002/tect.20069

Ault, A. K., Guenthner, W. R., Moser, A. C., Miller, G. H., and Refsnider, K. A., 2018, Zircon grain selection reveals (de)coupled metamictization, radiation damage, and He diffusivity: Chemical Geology, v. 490, p. 1–12, https://doi.org/10.1016/j.chemgeo.2018.04.023

Baughman, J. S., and Flowers, R. M., 2020, Mesoproterozoic burial of the Kaapvaal craton, southern Africa during Rodinia supercontinent assembly from (U-Th)/He thermochronology: Earth and Planetary Science Letters, v. 531, p. 115930, https://doi.org/10.1016/j.epsl.2019.115930

Berner, R. A., Lasaga, A. C., and Garrels, R. M., 1983, The Carbonate-Silicate Geochemical Cycle and Its Effect on Atmospheric Carbon-Dioxide over the Past 100 Million Years: American Journal of Science, v. 283, n. 7, p. 641–683, https://doi.org/10.2475/ajs.283.7.641

Blakey, R. C., Fielding, C. R., Frank, T. D., and Isbell, J. L., 2008, Gondwana paleogeography from assembly to breakup—A 500 m.y. odyssey, *in* Fielding, C. R., Frank, T. D., and Isbell, J. L., editors, Resolving the Late Paleozoic Ice Age in Time and Space, Special Paper, v. 441, Geological Society of America, https://doi.org/10.1130/2008.2441(01)

Bose, P. K., Sarkar, S., Chakrabarty, S., and Banerjee, S., 2001, Overview of the meso- to neoproterozoic evolution of the Vindhyan basin, central India: Sedimentary Geology, v. 141–142, p. 395–419, https://doi.org/10.1016/S0037-0738(01)00084-7

Bose, P. K., Sarkar, S., Das, N. G., Banerjee, S., Mandal, A., and Chakraborty, N., 2015, Proterozoic Vindhyan Basin: configuration and evolution, *in* Mazumder, R., and Eriksson, P. G., editors, Precambrian basins of India: stratigraphic and textonic context: Geological Society, London, Memoirs, v. 43, n. 1, Chapter 6, p. 85–102, https://doi.org/10.1144/M43.6

Chakrabarti, R., Basu, A. R., and Chakrabarti, A., 2007, Trace element and Nd-isotopic evidence for sediment sources in the mid-Proterozoic Vindhyan Basin, central India: Precambrian Research, v. 159, n. 3–4, p. 260–274, https://doi.org/10.1016/j.precamres.2007.07.003

Chakraborty, P. P., Pant, N. C., and Paul, P. P., 2015, Controls on sedimentation in Indian Palaeoproterozoic basins: clues from the Gwalior and Bijawar basins, central India, *in* Mazumder, R., and Eriksson, P. G., editors, Precambrian basins of India: stratigraphic and tectonic context: Geological Society, London, Memoirs, v. 43, n. 1, p. 67–83, https://doi.org/10.1144/M43.5

Cherniak, D. J., 2019, Diffusion of helium in radiation-damaged zircon: Chemical Geology, v. 529, p. 119308, https://doi.org/10.1016/j.chemgeo.2019.119308

Colleps, C. L., McKenzie, N. R., Stockli, D. F., Hughes, N. C., Singh, B. P., Webb, A. A. G., Myrow, P. M., Planavsky, N. J., and Horton, B. K., 2018, Zircon (U-Th)/He Thermochronometric Constraints on Himalayan Thrust Belt Exhumation, Bedrock Weathering, and Cenozoic Seawater Chemistry: Geochemistry, Geophysics, Geosystems, v. 19, n. 1, p. 257–271, https://doi.org/10.1002/2017GC007191

Colleps, C. L., McKenzie, N. R., Guenthner, W. R., Sharma, M., Gibson, T. M., and Stockli, D. F., 2021a, Apatite (U-Th)/He thermochronometric constraints on the northern extent of the Deccan large igneous province: Earth and Planetary Science Letters, v. 571, p. 117087, https://doi.org/10.1016/j.epsl.2021.117087

Colleps, C. L., McKenzie, N. R., Sharma, M., Liu, H., Gibson, T. M., Chen, W., and Stockli, D. F., 2021b, Zircon and apatite U-Pb age constraints from the Bundelkhand craton and Proterozoic strata of central India: Insights into craton stabilization and subsequent basin evolution: Precambrian Research, v. 362, p. 106286, https://doi.org/10.1016/j.precamres.2021.106286

Cooperdock, E. H. G., Ketcham, R. A., and Stockli, D. F., 2019, Resolving the effects of 2-D versus 3-D grain measurements on apatite (U–Th)/ He age data and reproducibility: Geochronology, v. 1, no. 1, p. 17–41, https://doi.org/10.5194/gchron-1-17-2019

Crawford, A. R., and Compston, W., 1969, The age of the Vindhyan System of Peninsular India: Quarterly Journal of the Geological Society, v. 125, n. 1–4, p. 351–371, https://doi.org/10.1144/gsjgs.125.1.0351

DeLucia, M. S., Guenthner, W. R., Marshak, S., Thomson, S. N., and Ault, A. K., 2017, Thermochronology links denudation of the Great Unconformity surface to the supercontinent cycle and snowball Earth: Geology, v. 48, n. 2, p. 167–170, https://doi.org/10.1130/G39525.1

Dodson, M. H., 1973, Closure Temperature in Cooling Geochronological and Petrological Systems: Contributions to Mineralogy and Petrology, v. 40, n. 3, p. 259–274, https://doi.org/10.1007/BF00373790

Dröllner, M., Barham, M., and Kirkland, C. L., 2022, Gaining from loss: Detrital zircon source-normalized α-dose discriminates first- versus multi-cycle grain histories: Earth and Planetary Science Letters, v. 579, p. 117346, https://doi.org/10.1016/j.epsl.2021.117346

Dutton, A., Rubin, K., McLean, N., Bowring, J., Bard, E., Edwards, R. L., Henderson, G. M., Reid, M. R., Richards, D. A., Sims, K. W. W., Walker, J. D., and Yokoyama, Y., 2017, Data reporting standards for publication of U-series data for geochronology and timescale assessment in the earth sciences: Quaternary Geochronology, v. 39, p. 142–149, https://doi.org/10.1016/j.quageo.2017.03.001

Farley, K. A., Wolf, R. A., and Silver, L. T., 1996, The effects of long alpha-stopping distances on (U-Th)/He ages: Geochimica Et Cosmochimica Acta, v. 60, n. 21, p. 4223–4229, https://doi.org/10.1016/S0016-7037(96)00193-7

Farley, K. A., Shuster, D., and Ketcham, R. A., 2011, U and Th zonation in apatite observed by laser ablation ICPMS, and implications for the (U–Th)/He system: Geochimica et Cosmochimica Acta, v. 75, n. 16, p. 4515–4530, https://doi.org/10.1016/j.gca.2011.05.020

Flowers, R. M., Shuster, D. L., Wernicke, B. P., and Farley, K. A., 2007, Radiation damage control on apatite (U-Th)/He dates from the Grand Canyon region, Colorado Plateau: Geology, v. 35, n. 5, p. 447–450, https://doi.org/10.1130/G23471A.1

Flowers, R. M., Ketcham, R. A., Shuster, D. L., and Farley, K. A., 2009, Apatite (U-Th)/He thermochronology using a radiation damage accumulation and annealing model: Geochimica et Cosmochimica Acta, v. 73, n. 8, p. 2347–2365, https://doi.org/10.1016/j.gca.2009.01.015

Flowers, R. M., Macdonald, F. A., Siddoway, C. S., and Havranek, R., 2020, Diachronous development of Great Unconformities before Neoproterozoic Snowball Earth: Proceedings of the National Academy of Sciences, v. 117, n. 19, p. 10172–10180, https://doi.org/10.1073/pnas.1913131117

Flowers, R. M., Ketcham, R. A., Macdonald, F. A., Siddoway, C. S., and Havranek, R. E., 2022, Existing thermochronologic data do not constrain Snowball glacial erosion below the Great Unconformities: Proceedings of the National Academy of Sciences, v. 119, n. 38, p. e2208451119, https://doi.org/10.1073/pnas.2208451119

Fox, M., and Shuster, D. L., 2014, The influence of burial heating on the (U–Th)/He system in apatite: Grand Canyon case study: Earth and Planetary Science Letters, v. 397, p. 174–183, https://doi.org/10.1016/j.epsl.2014.04.041

Fox, M., Dai, J.-G., and Carter, A., 2019, Badly Behaved Detrital (U-Th)/He Ages: Problems With He Diffusion Models or Geological Models?: Geochemistry, Geophysics, Geosystems, v. 20, n. 5, p. 2418–2432, https://doi.org/10.1029/2018GC008102

Gautheron, C., Tassan-Got, L., Barbarand, J., and Pagel, M., 2009, Effect of alpha-damage annealing on apatite (U–Th)/He thermochronology: Chemical Geology, v. 266, n. 3–4, p. 157–170, https://doi.org/10.1016/j.chemgeo.2009.06.001

Gautheron, C., Tassan-Got, L., Ketcham, R. A., and Dobson, K. J., 2012, Accounting for long alpha-particle stopping distances in (U–Th–Sm)/He geochronology: 3D modeling of diffusion, zoning, implantation, and abrasion: Geochimica et Cosmochimica Acta, v. 96, p. 44–56, https://doi.org/10.1016/j.gca.2012.08.016

Gautheron, C., Djimbi, D. M., Roques, J., Balout, H., Ketcham, R. A., Simoni, E., Pik, R., Seydoux-Guillaume, A.-M., and Tassan-Got, L., 2020, A multi-method, multi-scale theoretical study of He and Ne diffusion in zircon: Geochimica et Cosmochimica Acta, v. 268, p. 348–367, https://doi.org/10.1016/j.gca.2019.10.007

Ginster, U., Reiners, P. W., Nasdala, L., and Chanmuang, N, C., 2019, Annealing kinetics of radiation damage in zircon: Geochimica et Cosmochimica Acta, v. 249, p. 225–246, https://doi.org/10.1016/j.gca.2019.01.033

Gopalan, K., Kumar, A., Kumar, S., and Vijayagopal, B., 2013, Depositional history of the Upper Vindhyan succession, central India: Time constraints from Pb–Pb isochron ages of its carbonate components: Precambrian Research, v. 233, p. 108–117, https://doi.org/10.1016/j.precamres.2013.04.014

Green, P., and Duddy, I., 2018, Apatite (U-Th-Sm)/He thermochronology on the wrong side of the tracks: Chemical Geology, v. 488, p. 21–33, https://doi.org/10.1016/j.chemgeo.2018.04.028

Gregory, L. C., Meert, J. G., Pradhan, V., Pandit, M. K., Tamrat, E., and Malone, S. J., 2006, A paleomagnetic and geochronologic study of the Majhgawan kimberlite, India: Implications for the age of the Upper Vindhyan Supergroup: Precambrian Research, v. 149, n. 1–2, p. 65–75, https://doi.org/10.1016/j.precamres.2006.05.005

Guenthner, W. R., 2021, Implementation of an Alpha Damage Annealing Model for Zircon (U-Th)/He Thermochronology With Comparison to a Zircon Fission Track Annealing Model: Geochemistry, Geophysics, Geosystems, v. 22, n. 2, p. e2019GC008757, https://doi.org/10.1029/2019GC008757

Guenthner, W. R., Reiners, P. W., Ketcham, R. A., Nasdala, L., and Giester, G., 2013, Helium diffusion in natural zircon: Radiation damage anisotropy, and the interpretation of zircon (U-Th)/He thermochronology: American Journal of Science, v. 313, n. 3, p. 145–198, https://doi.org/10.2475/03.2013.01

Guenthner, W. R., Reiners, P. W., DeCelles, P. G., and Kendall, J., 2015, Sevier belt exhumation in central Utah constrained from complex zircon (U-Th)/He data sets: Radiation damage and He inheritance effects on partially reset detrital zircons: Geological Society of America Bulletin, v. 127, n. 3–4, p. 323–348, https://doi.org/10.1130/B31032.1

Guenthner, W. R., Reiners, P. W., and Chowdhury, U., 2016, Isotope dilution analysis of Ca and Zr in apatite and zircon (U-Th)/He chronometry: Geochemistry Geophysics Geosystems, v. 17, n. 5, p. 1623–1640, https://doi.org/10.1002/2016GC006311

Guenthner, W. R., Reiners, P. W., Drake, H., and Tillberg, M., 2017, Zircon, titanite, and apatite (U-Th)/He ages and age-eU correlations from the Fennoscandian Shield, southern Sweden: Tectonics, v. 36, n. 7, p. 1254–1274, https://doi.org/10.1002/2017TC004525

Hourigan, J. K., Reiners, P. W., and Brandon, M. T., 2005, U-Th zonation-dependent alpha-ejection in (U-Th)/He chronometry: Geochimica et Cosmochimica Acta, v. 69, n. 13, p. 3349–3365, https://doi.org/10.1016/j.gca.2005.01.024

Hueck, M., Dunkl, I., Heller, B., Stipp Basei, M. A., and Siegesmund, S., 2018, (U-Th)/He Thermochronology and Zircon Radiation Damage in the South American Passive Margin: Thermal Overprint of the Paraná LIP?: Tectonics, v. 37, n. 10, p. 4068–4085, https://doi.org/10.1029/2018TC005041

Isbell, J. L., Henry, L. C., Gulbranson, E. L., Limarino, C. O., Fraiser, M. L., Koch, Z. J., Ciccioli, P. L., and Dineen, A. A., 2012, Glacial paradoxes during the late Paleozoic ice age: Evaluating the equilibrium line altitude as a control on glaciation: Gondwana Research, v. 22, n. 1, p. 1–19, https://doi.org/10.1016/j.gr.2011.11.005

Johnson, J. E., Flowers, R. M., Baird, G. B., and Mahan, K. H., 2017, "Inverted" zircon and apatite (U–Th)/He dates from the Front Range, Colorado: High-damage zircon as a low-temperature (<50 °C) thermochronometer: Earth and Planetary Science Letters, v. 466, p. 80–90, https://doi.org/10.1016/j.epsl.2017.03.002

Joshi, K. B., Bhattacharjee, J., Rai, G., Halla, J., Ahmad, T., Kurhila, M., Heilimo, E., and Choudhary, A. K., 2017, The diversification of granitoids and plate tectonic implications at the Archaean–Proterozoic boundary in the Bundelkhand Craton, Central India: Geological Society, London, Special Publications, v. 449, n. 1, p. 123–157, https://doi.org/10.1144/SP449.8

Kaur, P., Zeh, A., and Chaudhri, N., 2014, Characterisation and U–Pb–Hf isotope record of the 3.55 Ga felsic crust from the Bundelkhand Craton, northern India: Precambrian Research, v. 255, p. 236–244, https://doi.org/10.1016/j.precamres.2014.09.019

Kaur, P., Zeh, A., Chaudhri, N., and Eliyas, N., 2016, Unravelling the record of Archaean crustal evolution of the Bundelkhand Craton, northern India using U–Pb zircon–monazite ages, Lu–Hf isotope systematics, and whole-rock geochemistry of granitoids: Precambrian Research, v. 281, p. 384–413, https://doi.org/10.1016/j.precamres.2016.06.005

Keller, C. B., Husson, J. M., Mitchell, R. N., Bottke, W. F., Gernon, T. M., Boehnke, P., Bell, E. A., Swanson-Hysell, N. L., and Peters, S. E., 2019, Neoproterozoic glacial origin of the Great Unconformity: Proceedings of the National Academy of Sciences, v. 116, n. 4, p. 1136–1145, https://doi.org/10.1073/pnas.1804350116

Ketcham, R. A., 2005, Forward and inverse modeling of low-temperature thermochronometry data: Reviews in Mineralogy and Geochemistry, v. 58, n. 1, p. 275–314, https://doi.org/10.2138/rmg.2005.58.11

Ketcham, R. A., Guenthner, W. R., and Reiners, P. W., 2013, Geometric analysis of radiation damage connectivity in zircon, and its implications for helium diffusion: American Mineralogist, v. 98, n. 2–3, p. 350–360, https://doi.org/10.2138/am.2013.4249

Kohn, B., and Gleadow, A., 2019, Application of Low-Temperature Thermochronology to Craton Evolution, *in* Malusà, M. G., and Fitzgerald, P. G., editors, Fission-Track Thermochronology and its Application to Geology: Cham: Springer International Publishing, p. 373–393, https://doi.org/10.1007/978-3-319-89421-8_21

Kumar, S., and Sharma, M., 2012, Vindhyan Basin, Son velley area, Central India: Palaeontological Society of India Field Guide Book, p. 1–145.

Lee, C.-T. A., Caves, J., Jiang, H., Cao, W., Lenardic, A., McKenzie, N. R., Shorttle, O., Yin, Q.-z., and Dyer, B., 2018, Deep mantle roots and continental emergence: implications for whole-Earth elemental cycling, long-term climate, and the Cambrian explosion: International Geology Review, v. 60, n. 4, p. 1–18, https://doi.org/10.1080/00206814.2017.1340853

Mackintosh, V., Kohn, B., Gleadow, A., and Tian, Y. T., 2017, Phanerozoic Morphotectonic Evolution of the Zimbabwe Craton: Unexpected Outcomes From a Multiple Low-Temperature Thermochronology Study: Tectonics, v. 36, n. 10, p. 2044–2067, https://doi.org/10.1002/2017TC004703

Malone, S. J., Meert, J. G., Banerjee, D. M., Pandit, M. K., Tamrat, E., Kamenov, G. D., Pradhan, V. R., and Sohl, L. E., 2008, Paleomagnetism and detrital zircon geochronology of the Upper Vindhyan sequence, Son Valley and Rajasthan, India: A ca. 1000 ma closure age for the Purana Basins?: Precambrian Research, v. 164, n. 3–4, p. 137–159, https://doi.org/10.1016/j.precamres.2008.04.004

McDannell, K. T., Zeitler, P. K., and Schneider, D. A., 2018, Instability of the southern Canadian Shield during the late Proterozoic: Earth and Planetary Science Letters, v. 490, p. 100–109, https://doi.org/10.1016/j.epsl.2018.03.012

McDannell, K. T., Schneider, D. A., Zeitler, P. K., O'Sullivan, P. B., and Issler, D. R., 2019, Reconstructing deep-time histories from integrated thermochronology: An example from southern Baffin Island, Canada: Terra Nova, v. 31, n. 3, p. 189–204, https://doi.org/10.1111/ter.12386

McDannell, K. T., Keller, C. B., Guenthner, W. R., Zeitler, P. K., and Shuster, D. L., 2022, Thermochronologic constraints on the origin of the Great Unconformity: Proceedings of the National Academy of Sciences, v. 119, n. 5, p. e2118682119, https://doi.org/10.1073/pnas.2118682119

McKenzie, N. R., Hughes, N. C., Myrow, P. M., Xiao, S. H., and Sharma, M., 2011, Correlation of Precambrian-Cambrian sedimentary successions across northern India and the utility of isotopic signatures of Himalayan lithotectonic zones: Earth and Planetary Science Letters, v. 312, n. 3–4, p. 471–483, https://doi.org/10.1016/j.epsl.2011.10.027

Meert, J. G., 2003, A synopsis of events related to the assembly of eastern Gondwana: Tectonophysics, v. 362, n. 1–4, p. 1–40, https://doi.org/10.1016/S0040-1951(02)00629-7

Meert, J., and Pandit, M., 2014, The Archean and Proterozoic History of Peninsular India: Tectonic Framework for Precambrian Sedimentary Basins in India: Geological Society, London, Memoirs, v. 43, p. 29–54, https://doi.org/10.1144/M43.3

Mishra, D. C., 2011, Long hiatus in Proterozoic sedimentation in India: Vindhyan, Cuddapah and Pakhal Basins—A plate tectonic model: Journal of the Geological Society of India, v. 77, n. 1, p. 17–25, https://doi.org/10.1007/s12594-011-0004-9

Mishra, D. C., 2015, Plume and Plate Tectonics Model for Formation of some Proterozoic Basins of India along Contemporary Mobile Belts: Mahakoshal — Bijawar, Vindhyan and Cuddapah Basins: Journal of the Geological Society of India, v. 85, n. 5, p. 525–536, https://doi.org/10.1007/s12594-015-0246-z

Montañez, I. P., and Poulsen, C. J., 2013, The Late Paleozoic ice age: an evolving paradigm: Annual Review of Earth and Planetary Sciences, v. 41, n. 1, p. 629–656, https://doi.org/10.1146/annurev.earth.031208.100118

Murray, K. E., Orme, D. A., and Reiners, P. W., 2014, Effects of U–Th-rich grain boundary phases on apatite helium ages: Chemical Geology, v. 390, p. 135–151, https://doi.org/10.1016/j.chemgeo.2014.09.023

Orme, D. A., Guenthner, W. R., Laskowski, A. K., and Reiners, P. W., 2016, Long-term tectonothermal history of Laramide basement from zircon-He age-eU correlations: Earth and Planetary Science Letters, v. 453, p. 119–130, https://doi.org/10.1016/j.epsl.2016.07.046

Peak, B. A., Flowers, R. M., Macdonald, F. A., and Cottle, J. M., 2021, Zircon (U-Th)/He thermochronology reveals pre-Great Unconformity paleotopography in the Grand Canyon region, USA: Geology, v. 49, n. 12, p. 1462–1466, https://doi.org/10.1130/G49116.1

Powell, J., Schneider, D., Stockli, D., and Fallas, K., 2016, Zircon (U-Th)/He thermochronology of Neoproterozoic strata from the Mackenzie Mountains, Canada: Implications for the Phanerozoic exhumation and deformation history of the northern Canadian Cordillera: Tectonics, v. 35, n. 3, p. 663–689, https://doi.org/10.1002/2015TC003989

Pujols, E. J., Stockli, D. F., Constenius, K. N., and Horton, B. K., 2020, Thermochronological and Geochronological Constraints on Late Cretaceous Unroofing and Proximal Sedimentation in the Sevier Orogenic Belt, Utah: Tectonics, v. 39, n. 7, p. e2019TC005794, https://doi.org/10.1029/2019TC005794

Ray, J. S., 2006, Age of the Vindhyan Supergroup: a review of recent findings: Journal of Earth System Science, v. 115, n. 1, p. 149–160, https://doi.org/10.1007/BF02703031

Reiners, P. W., 2009, Nonmonotonic thermal histories and contrasting kinetics of multiple thermochronometers: Geochimica et Cosmochimica Acta, v. 73, n. 12, p. 3612–3629, https://doi.org/10.1016/j.gca.2009.03.038

Reiners, P. W., Farley, K. A., and Hickes, H. J., 2002, He diffusion and (U-Th)/He thermochronometry of zircon: initial results from Fish Canyon Tuff and Gold Butte: Tectonophysics, v. 349, n. 1–4, p. 297–308, https://doi.org/10.1016/S0040-1951(02)00058-6

Reiners, P. W., Campbell, I. H., Nicolescu, S., Allen, C. M., Hourigan, J. K., Garver, J. I., Mattinson, J. M., and Cowan, D. S., 2005, (U-Th)/(HE-Pb) double dating of detrital zircons: American Journal of Science, v. 305, n. 4, p. 259–311, https://doi.org/10.2475/ajs.305.4.259

Rolland, Y., Bernet, M., van der Beek, P., Gautheron, C., Duclaux, G., Bascou, J., Balvay, M., Héraudet, L., Sue, C., and Ménot, R.-P., 2019, Late Paleozoic Ice Age glaciers shaped East Antarctica landscape: Earth and Planetary Science Letters, v. 506, p. 123–133, https://doi.org/10.1016/j.epsl.2018.10.044

Sarkar, S., Banerjee, S., Chakraborty, S., and Bose, P. K., 2002, Shelf storm flow dynamics: insight from the Mesoproterozoic Rampur Shale, central India: Sedimentary Geology, v. 147, n. 1–2, p. 89–104, https://doi.org/10.1016/S0037-0738(01)00189-0

Schöbel, S., de Wall, H., Ganerød, M., Pandit, M. K., and Rolf, C., 2014, Magnetostratigraphy and ^{40}Ar–^{39}Ar geochronology of the Malwa Plateau region (Northern Deccan Traps), central western India: Significance and correlation with the main Deccan Large Igneous Province sequences: Journal of Asian Earth Sciences, v. 89, p. 28–45, https://doi.org/10.1016/j.jseaes.2014.03.022

Schoene, B., Samperton, K. M., Eddy, M. P., Keller, G., Adatte, T., Bowring, S. A., Khadri, S. F. R., and Gertsch, B., 2015, U-Pb geochronology of the Deccan Traps and relation to the end-Cretaceous mass extinction: Science, v. 347, n. 6218, p. 182–184, https://doi.org/10.1126/science.aaa0118

Shukla, A. D., George, B. G., and Ray, J. S., 2019, Evolution of the Proterozoic Vindhyan Basin, Rajasthan, India: insights from geochemical provenance of siliciclastic sediments: International Geology Review, v. 62, n. 2, p. 153–167, https://doi.org/10.1080/00206814.2019.1594412

Shuster, D. L., and Farley, K. A., 2009, The influence of artificial radiation damage and thermal annealing on helium diffusion kinetics in apatite: Geochimica et Cosmochimica Acta, v. 73, n. 1, p. 183–196, https://doi.org/10.1016/j.gca.2008.10.013

Shuster, D. L., Flowers, R. M., and Farley, K. A., 2006, The influence of natural radiation damage on helium diffusion kinetics in apatite: Earth and Planetary Science Letters, v. 249, n. 3–4, p. 148–161, https://doi.org/10.1016/j.epsl.2006.07.028

Slabunov, A. I., and Singh, V. K., 2019, Meso–Neoarchaean crustal evolution of the Bundelkhand Craton, Indian Shield: new data from greenstone belts: International Geology Review, v. 61, n. 11, p. 1409–1428, https://doi.org/10.1080/00206814.2018.1512906

Sobolev, S. V., and Brown, M., 2019, Surface erosion events controlled the evolution of plate tectonics on Earth: Nature, v. 570, n. 7759, p. 52–57, https://doi.org/10.1038/s41586-019-1258-4

Sprain, C. J., Renne, P. R., Vanderkluysen, L., Pande, K., Self, S., and Mittal, T., 2019, The eruptive tempo of Deccan volcanism in relation to the Cretaceous-Paleogene boundary: Science, v. 363, n. 6429, p. 866–870, https://doi.org/10.1126/science.aav1446

Stampfli, G. M., and Borel, G. D., 2002, A plate tectonic model for the Paleozoic and Mesozoic constrained by dynamic plate boundaries and restored synthetic oceanic isochrons: Earth and Planetary Science Letters, v. 196, n. 1–2, p. 17–33, https://doi.org/10.1016/S0012-821X(01)00588-X

Stern, R. J., 1994, Arc assembly and continental collision in the Neoproterozoic East African Orogen: implications for the consolidation of Gondwanaland: Annual Review of Earth and Planetary Sciences, v. 22, p. 319–351, https://doi.org/10.1146/annurev.ea.22.050194.001535

Thurston, O. G., Guenthner, W. R., Karlstrom, K. E., Ricketts, J. W., Heizler, M. T., and Timmons, J. M., 2022, Zircon (U-Th)/He thermochronology of Grand Canyon resolves 1250 Ma unroofing at the Great Unconformity and< 20 Ma canyon carving: Geology, v. 50, n. 2, p. 222–226, https://doi.org/10.1130/G48699.1

Turner, C. C., Meert, J. G., Pandit, M. K., and Kamenov, G. D., 2014, A detrital zircon U–Pb and Hf isotopic transect across the Son Valley sector of the Vindhyan Basin, India: Implications for basin evolution and paleogeography: Gondwana Research, v. 26, n. 1, p. 348–364, https://doi.org/10.1016/j.gr.2013.07.009

Upadhyay, R., Gautam, S., and Awatar, R., 2022, Discovery of an Entrapped Early Permian (ca. 299 Ma) Peri-Gondwanic Sliver in the Cretaceous Shyok Suture of Northern Ladakh, India: Diverse Implications: GSA Today, v. 32, n. 1https://doi.org/10.1130/GSATG481A.1

Verma, A., and Shukla, U. K., 2015, Deposition of the Upper Rewa Sandstone Formation of proterozoic Rewa group of the Vindhyan Basin, M.P., India: A Reappraisal: Journal of the Geological Society of India, v. 86, n. 4, p. 421–437, https://doi.org/10.1007/s12594-015-0330-4

Willett, C. D., Fox, M., and Shuster, D. L., 2017, A helium-based model for the effects of radiation damage annealing on helium diffusion kinetics in apatite: Earth and Planetary Science Letters, v. 477, p. 195–204, https://doi.org/10.1016/j.epsl.2017.07.047

Wolfe, M. R., and Stockli, D. F., 2010, Zircon (U-Th)/He thermochronometry in the KTB drill hole, Germany, and its implications for bulk He diffusion kinetics in zircon: Earth and Planetary Science Letters, v. 295, n. 1–2, p. 69–82, https://doi.org/10.1016/j.epsl.2010.03.025

Zeitler, P. K., Herczeg, A. L., Mcdougall, I., and Honda, M., 1987, U-Th-He Dating of Apatite - a Potential Thermochronometer: Geochimica Et Cosmochimica Acta, v. 51, n. 10, p. 2865-2868, https://doi.org/10.1016/0016-7037(87)90164-5

Zhang, N., Zhong, S., and Flowers, R. M., 2012, Predicting and testing continental vertical motion histories since the Paleozoic: Earth and Planetary Science Letters, v. 317–318, p. 426–435, https://doi.org/10.1016/j.epsl.2011.10.041